

# Exclusive photoproduction of $J/\psi$ mesons at HERA

ZEUS Collaboration

## Abstract

The exclusive photoproduction of  $J/\psi$  mesons,  $\gamma p \rightarrow J/\psi p$ , has been studied in  $ep$  collisions with the ZEUS detector at HERA, in the kinematic range  $20 < W < 290$  GeV, where  $W$  is the photon-proton centre-of-mass energy. The  $J/\psi$  mesons were reconstructed in the muon and the electron decay channels using integrated luminosities of  $38 \text{ pb}^{-1}$  and  $55 \text{ pb}^{-1}$ , respectively. The helicity structure of  $J/\psi$  production shows that the hypothesis of  $s$ -channel helicity conservation is satisfied within two standard deviations. The total cross section and the differential cross-section  $d\sigma/dt$ , where  $t$  is the squared four-momentum transfer at the proton vertex, are presented as a function of  $W$ , for  $|t| < 1.8 \text{ GeV}^2$ . The  $t$  distribution exhibits an exponential shape with a slope parameter increasing logarithmically with  $W$  with a value  $b = 4.15 \pm 0.05(\text{stat.})_{-0.18}^{+0.30}(\text{syst.}) \text{ GeV}^{-2}$  at  $W = 90 \text{ GeV}$ . The effective parameters of the Pomeron trajectory are  $\alpha_P(0) = 1.200 \pm 0.009(\text{stat.})_{-0.010}^{+0.004}(\text{syst.})$  and  $\alpha'_P = 0.115 \pm 0.018(\text{stat.})_{-0.015}^{+0.008}(\text{syst.}) \text{ GeV}^{-2}$ .

# The ZEUS Collaboration

S. Chekanov, D. Krakauer, S. Magill, B. Musgrave, A. Pellegrino, J. Repond, R. Yoshida  
*Argonne National Laboratory, Argonne, Illinois 60439-4815<sup>n</sup>*

M.C.K. Mattingly

*Andrews University, Berrien Springs, Michigan 49104-0380*

P. Antonioli, G. Bari, M. Basile, L. Bellagamba, D. Boscherini, A. Bruni, G. Bruni,  
G. Cara Romeo, L. Cifarelli, F. Cindolo, A. Contin, M. Corradi, S. De Pasquale, P. Giusti,  
G. Iacobucci, G. Levi, A. Margotti, T. Massam, R. Nania, F. Palmonari, A. Pesci, G. Sar-  
torelli, A. Zichichi

*University and INFN Bologna, Bologna, Italy<sup>e</sup>*

G. Aghuzumtsyan, D. Bartsch, I. Brock, J. Crittenden<sup>1</sup>, S. Goers, H. Hartmann, E. Hilger,  
P. Irrgang, H.-P. Jakob, A. Kappes, U.F. Katz<sup>2</sup>, R. Kerger, O. Kind, E. Paul, J. Rautenberg<sup>3</sup>,  
R. Renner, H. Schnurbusch, A. Stifutkin, J. Tandler, K.C. Voss, A. Weber, H. Wessoleck  
*Physikalisches Institut der Universität Bonn, Bonn, Germany<sup>b</sup>*

D.S. Bailey<sup>4</sup>, N.H. Brook<sup>4</sup>, J.E. Cole, B. Foster, G.P. Heath, H.F. Heath, S. Robins,  
E. Rodrigues<sup>5</sup>, J. Scott, R.J. Tapper, M. Wing

*H.H. Wills Physics Laboratory, University of Bristol, Bristol, United Kingdom<sup>m</sup>*

M. Capua, A. Mastroberardino, M. Schioppa, G. Susinno

*Calabria University, Physics Department and INFN, Cosenza, Italy<sup>e</sup>*

J.Y. Kim, Y.K. Kim, J.H. Lee, I.T. Lim, M.Y. Pac<sup>6</sup>

*Chonnam National University, Kwangju, Korea<sup>9</sup>*

A. Caldwell, M. Helbich, X. Liu, B. Mellado, S. Paganis, W.B. Schmidke, F. Sciulli  
*Nevis Laboratories, Columbia University, Irvington on Hudson, New York 10027<sup>o</sup>*

J. Chwastowski, A. Eskreys, J. Figiel, K. Olkiewicz, M.B. Przybycień<sup>7</sup>, P. Stopa, L. Za-  
wiejski

*Institute of Nuclear Physics, Cracow, Poland<sup>i</sup>*

B. Bednarek, I. Grabowska-Bold, K. Jeleń, D. Kisielewska, A.M. Kowal<sup>8</sup>, M. Kowal,  
T. Kowalski, B. Mindur, M. Przybycień, E. Rulikowska-Zarebska, L. Suszycki, D. Szuba,  
J. Szuba<sup>9</sup>

*Faculty of Physics and Nuclear Techniques, University of Mining and Metallurgy, Cracow,  
Poland<sup>i</sup>*

A. Kotański, W. Słomiński<sup>10</sup>

*Department of Physics, Jagellonian University, Cracow, Poland*

L.A.T. Bauerdick<sup>11</sup>, U. Behrens, K. Borrás, V. Chiochia, D. Dannheim, M. Derrick<sup>12</sup>, K. Desler<sup>13</sup>, G. Drews, J. Fourletova, A. Fox-Murphy, U. Fricke, A. Geiser, F. Goebel, P. Göttlicher<sup>14</sup>, R. Graciani, T. Haas, W. Hain, G.F. Hartner, S. Hillert, U. Kötz, H. Kowalski, H. Labes, D. Lelas, B. Löhr, R. Mankel, M. Martínez<sup>11</sup>, M. Moritz, D. Notz, M.C. Petrucci, A. Polini, U. Schneekloth, F. Selonke, B. Surrow<sup>15</sup>, R. Wichmann<sup>16</sup>, G. Wolf, C. Youngman, W. Zeuner

*Deutsches Elektronen-Synchrotron DESY, Hamburg, Germany*

A. Lopez-Duran Viani, A. Meyer, S. Schlenstedt

*DESY Zeuthen, Zeuthen, Germany*

G. Barbagli, E. Gallo, C. Genta, P. G. Pelfer

*University and INFN, Florence, Italy<sup>e</sup>*

A. Bamberger, A. Benen, N. Coppola, P. Markun, H. Raach, S. Wölflé

*Fakultät für Physik der Universität Freiburg i.Br., Freiburg i.Br., Germany<sup>b</sup>*

M. Bell, P.J. Bussey, A.T. Doyle, C. Glasman, S. Hanlon, S.W. Lee, A. Lupi, G.J. McCance, D.H. Saxon, I.O. Skillicorn

*Department of Physics and Astronomy, University of Glasgow, Glasgow, United Kingdom<sup>m</sup>*

B. Bodmann, U. Holm, H. Salehi, K. Wick, A. Ziegler, Ar. Ziegler

*Hamburg University, I. Institute of Exp. Physics, Hamburg, Germany<sup>b</sup>*

T. Carli, I. Gialas<sup>17</sup>, K. Klimek, E. Lohrmann, M. Milite, S. Stonjek<sup>18</sup>,

*Hamburg University, II. Institute of Exp. Physics, Hamburg, Germany<sup>b</sup>*

C. Collins-Tooth, C. Foudas, R. Gonçalo<sup>5</sup>, K.R. Long, F. Metlica, D.B. Miller, A.D. Tapper, R. Walker

*Imperial College London, High Energy Nuclear Physics Group, London, United Kingdom<sup>m</sup>*

P. Cloth, D. Filges

*Forschungszentrum Jülich, Institut für Kernphysik, Jülich, Germany*

M. Kuze, K. Nagano, K. Tokushuku<sup>19</sup>, S. Yamada, Y. Yamazaki

*Institute of Particle and Nuclear Studies, KEK, Tsukuba, Japan<sup>f</sup>*

A.N. Barakbaev, E.G. Boos, N.S. Pokrovskiy, B.O. Zhautykov

*Institute of Physics and Technology of Ministry of Education and Science of Kazakhstan, Almaty, Kazakhstan*

S.H. Ahn, S.B. Lee, S.K. Park

*Korea University, Seoul, Korea<sup>g</sup>*

H. Lim, D. Son

*Kyungpook National University, Taegu, Korea <sup>g</sup>*

F. Barreiro, G. García, O. González, L. Labarga, J. del Peso, I. Redondo<sup>20</sup>, J. Terrón,  
M. Vázquez

*Departamento de Física Teórica, Universidad Autónoma Madrid, Madrid, Spain <sup>l</sup>*

M. Barbi, A. Bertolin, F. Corriveau, A. Ochs, S. Padhi, D.G. Stairs, M. St-Laurent  
*Department of Physics, McGill University, Montréal, Québec, Canada H3A 2T8 <sup>a</sup>*

T. Tsurugai

*Meiji Gakuin University, Faculty of General Education, Yokohama, Japan*

A. Antonov, V. Bashkirov<sup>21</sup>, P. Danilov, B.A. Dolgoshein, D. Gladkov, V. Sosnovtsev,  
S. Suchkov

*Moscow Engineering Physics Institute, Moscow, Russia <sup>j</sup>*

R.K. Dementiev, P.F. Ermolov, Yu.A. Golubkov, I.I. Katkov, L.A. Khein, N.A. Korotkova,  
I.A. Korzhavina, V.A. Kuzmin, B.B. Levchenko, O.Yu. Lukina, A.S. Proskuryakov, L.M. Shche-  
glova, A.N. Solomin, N.N. Vlasov, S.A. Zotkin

*Moscow State University, Institute of Nuclear Physics, Moscow, Russia <sup>k</sup>*

C. Bokel, J. Engelen, S. Grijpink, E. Koffeman, P. Kooijman, E. Maddox, S. Schagen,  
E. Tassi, H. Tiecke, N. Tuning, J.J. Velthuis, L. Wiggers, E. de Wolf

*NIKHEF and University of Amsterdam, Amsterdam, Netherlands <sup>h</sup>*

N. Brümmner, B. Bylsma, L.S. Durkin, J. Gilmore, C.M. Ginsburg, C.L. Kim, T.Y. Ling  
*Physics Department, Ohio State University, Columbus, Ohio 43210 <sup>n</sup>*

S. Boogert, A.M. Cooper-Sarkar, R.C.E. Devenish, J. Ferrando, T. Matsushita, M. Rigby,  
O. Ruske<sup>22</sup>, M.R. Sutton, R. Walczak

*Department of Physics, University of Oxford, Oxford United Kingdom <sup>m</sup>*

R. Brugnera, R. Carlin, F. Dal Corso, S. Dusini, A. Garfagnini, S. Limentani, A. Longhin,  
A. Parenti, M. Posocco, L. Stanco, M. Turcato

*Dipartimento di Fisica dell' Università and INFN, Padova, Italy <sup>e</sup>*

L. Adamczyk<sup>23</sup>, E.A. Heaphy, B.Y. Oh, P.R.B. Saull<sup>23</sup>, J.J. Whitmore

*Department of Physics, Pennsylvania State University, University Park, Pennsylvania  
16802 <sup>o</sup>*

Y. Iga

*Polytechnic University, Sagamihara, Japan <sup>f</sup>*

G. D'Agostini, G. Marini, A. Nigro

*Dipartimento di Fisica, Università 'La Sapienza' and INFN, Rome, Italy <sup>e</sup>*

C. Cormack, J.C. Hart, N.A. McCubbin  
*Rutherford Appleton Laboratory, Chilton, Didcot, Oxon, United Kingdom*<sup>m</sup>

C. Heusch  
*University of California, Santa Cruz, California 95064*<sup>n</sup>

I.H. Park  
*Seoul National University, Seoul, Korea*

N. Pavel  
*Fachbereich Physik der Universität-Gesamthochschule Siegen, Germany*

H. Abramowicz, S. Dagan, A. Gabareen, S. Kananov, A. Kreisel, A. Levy  
*Raymond and Beverly Sackler Faculty of Exact Sciences, School of Physics, Tel-Aviv University, Tel-Aviv, Israel*<sup>d</sup>

T. Abe, T. Fusayasu, T. Kohno, K. Umemori, T. Yamashita  
*Department of Physics, University of Tokyo, Tokyo, Japan*<sup>f</sup>

R. Hamatsu, T. Hirose, M. Inuzuka, S. Kitamura<sup>24</sup>, K. Matsuzawa, T. Nishimura  
*Tokyo Metropolitan University, Department of Physics, Tokyo, Japan*<sup>f</sup>

M. Arneodo<sup>25</sup>, N. Cartiglia, R. Cirio, M. Costa, M.I. Ferrero, S. Maselli, V. Monaco, C. Peroni, M. Ruspa, R. Sacchi, A. Solano, A. Staiano  
*Università di Torino, Dipartimento di Fisica Sperimentale and INFN, Torino, Italy*<sup>e</sup>

R. Galea, T. Koop, G.M. Levman, J.F. Martin, A. Mirea, A. Sabetfakhri  
*Department of Physics, University of Toronto, Toronto, Ontario, Canada M5S 1A7*<sup>a</sup>

J.M. Butterworth, C. Gwenlan, R. Hall-Wilton, T.W. Jones, J.B. Lane, M.S. Lightwood, J.H. Loizides<sup>26</sup>, B.J. West  
*Physics and Astronomy Department, University College London, London, United Kingdom*<sup>m</sup>

J. Ciborowski<sup>27</sup>, R. Ciesielski, G. Grzelak, R.J. Nowak, J.M. Pawlak, B. Smalska<sup>28</sup>, J. Sztuk<sup>29</sup>, T. Tymieniecka<sup>30</sup>, A. Ukleja<sup>30</sup>, J. Ukleja, J.A. Zakrzewski, A.F. Żarnecki  
*Warsaw University, Institute of Experimental Physics, Warsaw, Poland*<sup>i</sup>

M. Adamus, P. Plucinski  
*Institute for Nuclear Studies, Warsaw, Poland*<sup>i</sup>

Y. Eisenberg, L.K. Gladilin<sup>31</sup>, D. Hochman, U. Karshon  
*Department of Particle Physics, Weizmann Institute, Rehovot, Israel*<sup>c</sup>

D. Kçira, S. Lammers, D.D. Reeder, A.A. Savin, W.H. Smith  
*Department of Physics, University of Wisconsin, Madison, Wisconsin 53706*<sup>n</sup>

A. Deshpande, S. Dhawan, V.W. Hughes, P.B. Straub  
*Department of Physics, Yale University, New Haven, Connecticut 06520-8121 <sup>n</sup>*

S. Bhadra, C.D. Catterall, S. Fourletov, S. Menary, M. Soares, J. Standage  
*Department of Physics, York University, Ontario, Canada M3J 1P3 <sup>a</sup>*

- <sup>1</sup> now at Cornell University, Ithaca/NY, USA
- <sup>2</sup> on leave of absence at University of Erlangen-Nürnberg, Germany
- <sup>3</sup> supported by the GIF, contract I-523-13.7/97
- <sup>4</sup> PPARC Advanced fellow
- <sup>5</sup> supported by the Portuguese Foundation for Science and Technology (FCT)
- <sup>6</sup> now at Dongshin University, Naju, Korea
- <sup>7</sup> now at Northwestern Univ., Evanston/IL, USA
- <sup>8</sup> supported by the Polish State Committee for Scientific Research, grant no. 5 P-03B 13720
- <sup>9</sup> partly supported by the Israel Science Foundation and the Israel Ministry of Science
- <sup>10</sup> Department of Computer Science, Jagellonian University, Cracow
- <sup>11</sup> now at Fermilab, Batavia/IL, USA
- <sup>12</sup> on leave from Argonne National Laboratory, USA
- <sup>13</sup> now at DESY group MPY
- <sup>14</sup> now at DESY group FEB
- <sup>15</sup> now at Brookhaven National Lab., Upton/NY, USA
- <sup>16</sup> now at Mobilcom AG, Rendsburg-Büdelndorf, Germany
- <sup>17</sup> Univ. of the Aegean, Greece
- <sup>18</sup> supported by NIKHEF, Amsterdam/NL
- <sup>19</sup> also at University of Tokyo
- <sup>20</sup> now at LPNHE Ecole Polytechnique, Paris, France
- <sup>21</sup> now at Loma Linda University, Loma Linda, CA, USA
- <sup>22</sup> now at IBM Global Services, Frankfurt/Main, Germany
- <sup>23</sup> partly supported by Tel Aviv University
- <sup>24</sup> present address: Tokyo Metropolitan University of Health Sciences, Tokyo 116-8551, Japan
- <sup>25</sup> also at Università del Piemonte Orientale, Novara, Italy
- <sup>26</sup> supported by Argonne National Laboratory, USA
- <sup>27</sup> also at Łódź University, Poland
- <sup>28</sup> supported by the Polish State Committee for Scientific Research, grant no. 2 P-03B 00219
- <sup>29</sup> Łódź University, Poland
- <sup>30</sup> sup. by Pol. State Com. for Scien. Res., 5 P-03B 09820 and by Germ. Fed. Min. for Edu. and Research (BMBF), POL 01/043
- <sup>31</sup> on leave from MSU, partly supported by University of Wisconsin via the U.S.-Israel BSF

- <sup>a</sup> supported by the Natural Sciences and Engineering Research Council of Canada (NSERC)
- <sup>b</sup> supported by the German Federal Ministry for Education and Research (BMBF), under contract numbers HZ1GUA 2, HZ1GUB 0, HZ1PDA 5, HZ1VFA 5
- <sup>c</sup> supported by the MINERVA Gesellschaft für Forschung GmbH, the Israel Science Foundation, the U.S.-Israel Binational Science Foundation, the Israel Ministry of Science and the Benozvio Center for High Energy Physics
- <sup>d</sup> supported by the German-Israeli Foundation, the Israel Science Foundation, and by the Israel Ministry of Science
- <sup>e</sup> supported by the Italian National Institute for Nuclear Physics (INFN)
- <sup>f</sup> supported by the Japanese Ministry of Education, Science and Culture (the Monbusho) and its grants for Scientific Research
- <sup>g</sup> supported by the Korean Ministry of Education and Korea Science and Engineering Foundation
- <sup>h</sup> supported by the Netherlands Foundation for Research on Matter (FOM)
- <sup>i</sup> supported by the Polish State Committee for Scientific Research, grant no. 115/E-343/SPUB-M/DESY/P-03/DZ 121/2001-2002
- <sup>j</sup> partially supported by the German Federal Ministry for Education and Research (BMBF)
- <sup>k</sup> supported by the Fund for Fundamental Research of Russian Ministry for Science and Education and by the German Federal Ministry for Education and Research (BMBF)
- <sup>l</sup> supported by the Spanish Ministry of Education and Science through funds provided by CICYT
- <sup>m</sup> supported by the Particle Physics and Astronomy Research Council, UK
- <sup>n</sup> supported by the US Department of Energy
- <sup>o</sup> supported by the US National Science Foundation



# 1 Introduction

Exclusive  $J/\psi$  photoproduction is expected to be described by models based on perturbative QCD (pQCD), since the mass of the charm quark provides a hard scale [1–9]. In such models, the photon fluctuates into a  $c\bar{c}$  pair which subsequently interacts with the proton. This interaction is modelled by the exchange of a gluon ladder and the cross section is proportional to the square of the gluon density. These models predict a rapid rise in the cross section with  $W$ , where  $W$  is the photon-proton centre-of-mass energy, which is caused by the fast increase of the gluon density in the proton at the small values of Bjorken  $x$ .

Within the framework of Regge phenomenology [10], diffractive interactions at large centre-of-mass energies are the result of the  $t$ -channel exchange of the Pomeron trajectory,  $\alpha_P(t)$ , carrying the quantum numbers of the vacuum. The differential cross section at high energies is expressed as

$$\frac{d\sigma}{dt} \propto F(t) \cdot W^{4[\alpha_P(t)-1]}, \quad (1)$$

where  $t$  is the squared four-momentum transfer at the proton vertex and  $F(t)$  is a function of  $t$  only. If  $d\sigma/dt$  decreases exponentially and the trajectory is linear in  $t$ ,  $\alpha_P(t) = \alpha_P(0) + \alpha'_P t$ , the cross section can be expressed as

$$\frac{d\sigma}{dt} \propto W^{4[\alpha_P(0)-1]} \cdot e^{b(W)t}, \quad (2)$$

where the slope parameter is  $b(W) = b_0 + 4\alpha'_P \ln(W/W_0)$  and  $W_0$  is an arbitrary energy scale parameter. A fit to hadronic data [11] yields the soft-Pomeron parameter  $\alpha'_P = 0.25 \text{ GeV}^{-2}$ . The pQCD models predict the effective  $\alpha'_P$  in the perturbative regime [2, 6, 12, 13] to be much smaller than  $0.25 \text{ GeV}^2$ .

Studies of the exclusive, diffractive photoproduction of vector charmonium states, i.e.  $\gamma p \rightarrow J/\psi p$ , at HERA show that the total cross section [14, 15] rises steeply with  $W$ . In addition, the  $t$  dependence of the cross section can be fitted by a single exponential,  $d\sigma/dt \sim e^{-b|t|}$ , with  $b \sim 4.6 \text{ GeV}^{-2}$  [14, 15]. There are indications that the slope parameter  $b$  has little variation with  $W$  [15, 16], i.e. little “shrinkage” is observed.

In this paper, more precise measurements of the  $t$  and  $W$  dependence of the exclusive photoproduction cross section  $J/\psi$  mesons are made using the reaction  $ep \rightarrow e\gamma p \rightarrow eJ/\psi p$  for values of the photon virtuality,  $Q^2$ , close to zero in the range  $20 < W < 290 \text{ GeV}$ . With respect to the previous ZEUS result [14], this analysis covers wider ranges in  $W$  and  $t$  and has a large increase in statistics, combined with an improved understanding of the detector and of the background subtraction. The cross section for  $\gamma p \rightarrow J/\psi p$  and the slope of the differential cross-section  $d\sigma_{\gamma p \rightarrow J/\psi p}/dt$  are studied as a function of  $W$ .

The Pomeron trajectory parameters  $\alpha_{\mathbb{P}}(0)$  and  $\alpha'_{\mathbb{P}}$ , which describe the  $W$  dependence of the cross section and the shrinkage, respectively, are determined. The helicity structure of  $J/\psi$  production is investigated to test the validity of SCHC.

## 2 Experimental set-up

In this analysis,  $J/\psi$  mesons were identified with the ZEUS detector at HERA by their decays to  $\mu^+\mu^-$  or to  $e^+e^-$ . The muon sample corresponds to an integrated luminosity of  $38.0 \pm 0.6 \text{ pb}^{-1}$ , collected in 1996 and 1997 when 27.5 GeV positrons<sup>1</sup> were collided with 820 GeV protons. For the measurement with  $20 < W < 30 \text{ GeV}$ , a sample from an integrated luminosity of  $27.5 \pm 0.4 \text{ pb}^{-1}$  was used. The electron sample corresponds to an integrated luminosity of  $55.2 \pm 1.2 \text{ pb}^{-1}$ , collected in 1999 and 2000 in collisions of 27.5 GeV positrons with 920 GeV protons.

The ZEUS detector is described in detail elsewhere [17]; only the components most relevant for this analysis are outlined here.

Charged particles are tracked by the central tracking detector (CTD) [18], which operates in a magnetic field of 1.43 T provided by a thin super-conducting coil. The CTD consists of 72 cylindrical drift chamber layers, organised in 9 superlayers covering the polar-angle<sup>2</sup> region  $15^\circ < \theta < 164^\circ$ . The relative transverse-momentum resolution for full-length tracks is  $\sigma(p_T)/p_T = 0.0058p_T \oplus 0.0065 \oplus 0.0014/p_T$ , with  $p_T$  in GeV.

Charged particles in the forward direction are detected in the forward tracking detector (FTD) [17], which consists of three planar drift chambers perpendicular to the beam covering the polar angles  $7^\circ < \theta < 28^\circ$ . Each chamber is made of three layers of drift cells; the wire directions in the second layer are rotated by  $120^\circ$  with respect to the first layer and similarly for the third layer with respect to the second. Each drift cell has six sense wires. Thus each chamber measures a track segment in three projections with up to six hits per projection.

Surrounding the solenoid is the high-resolution uranium-scintillator calorimeter (CAL) [19]. It consists of three parts: the forward (FCAL,  $2.6^\circ < \theta < 36.7^\circ$ ), the barrel (BCAL,

---

<sup>1</sup> Hereafter, “positron” is used to refer to both electron and positron beams. At the values of  $Q^2$  studied here,  $e^-p$  and  $e^+p$  scattering were assumed to give identical results since contributions from  $Z^0$  exchange are negligible. Similarly, “electron” is used to refer to either the electron or positron from the decay of the  $J/\psi$ .

<sup>2</sup> The ZEUS coordinate system is a right-handed Cartesian system, with the  $Z$ -axis pointing in the proton beam direction, referred to as the “forward direction”, and the  $X$ -axis pointing left towards the centre of HERA. The coordinate origin is at the nominal interaction point. The pseudorapidity is defined as  $\eta = -\ln(\tan \frac{\theta}{2})$ , where the polar angle,  $\theta$ , is measured with respect to the proton beam direction.

$36.7^\circ < \theta < 129.1^\circ$ ) and the rear (RCAL,  $129.1^\circ < \theta < 176.2^\circ$ ) calorimeters. Each part is subdivided transversely into towers and longitudinally into one electromagnetic section (EMC) and either one (in RCAL) or two (in BCAL and FCAL) hadronic sections (HAC). The smallest subdivision of the calorimeter is called a cell. Under test beam conditions, the CAL has relative energy resolutions of  $\sigma(E)/E = 0.18/\sqrt{E}$  for electrons hitting the center of a calorimeter cell and  $\sigma(E)/E = 0.35/\sqrt{E}$  for single hadrons ( $E$  in GeV). Cell clusters were used to aid in the identification of muons and electrons.

The forward plug calorimeter (FPC) [20] is a lead-scintillator sandwich calorimeter with wavelength-shifter fibre readout. Installed in 1998 in the  $20 \times 20$  cm<sup>2</sup> beamhole of the FCAL, it has a small hole of radius 3.15 cm in the centre to accommodate the beampipe. It extends the pseudorapidity coverage of the forward calorimeter from  $\eta < 4.0$  to  $\eta < 5.0$ .

The small-angle rear tracking detector (SRTD) [21] is attached to the front face of the RCAL. The SRTD consists of two planes of scintillator strips read out via optical fibres and photomultiplier tubes. It covers the region  $68 \times 68$  cm<sup>2</sup> in  $X$  and  $Y$  with the exclusion of a  $8 \times 20$  cm<sup>2</sup> hole at the centre for the beampipe. The SRTD provides a transverse position resolution of 3 mm and was used to measure the positions of electrons, from the  $J/\psi$  decay, produced at small angles to the positron beam direction.

The muon system consists of limited streamer tubes (forward, barrel and rear muon chambers: FMUON [17], B/RMUON [22]) placed inside and outside the magnet yoke. The inner chambers, F/B/RMUI, cover the polar angles between  $10^\circ < \theta < 35^\circ$ ,  $34^\circ < \theta < 135^\circ$  and  $135^\circ < \theta < 171^\circ$ , respectively. The FMUON has additional drift chambers and permits high-momentum muon reconstruction for polar angles between  $6^\circ$  and  $30^\circ$  using the magnetic field of 1.7 T produced by two iron toroids placed at  $Z = 9$  m and the toroidal field of 1.6 T provided by the yoke coils. The relative momentum resolution of  $\sigma(p)/p = 0.2$ , up to 20 GeV, is dominated by the multiple scattering.

The proton-remnant tagger (PRT1) [23] consists of two layers of scintillation counters located at  $Z = 5.15$  m, and covers the pseudorapidity range  $4.3 < \eta < 5.8$ . It was used, up to the end of the 1997 running period, to tag events in which the proton diffractively dissociates.

The luminosity was determined from the rate of the bremsstrahlung process  $ep \rightarrow e\gamma p$ , where the photon was measured with a lead-scintillator calorimeter [24] located at  $Z = -107$  m.

### 3 Kinematic variables and reconstruction

The kinematic variables used to describe exclusive  $J/\psi$  production,

$$e(k) p(P) \rightarrow e(k') J/\psi(v) p(P'),$$

where  $k, k', P, P'$  and  $v$  are the four-momenta of the incident positron, scattered positron, incident proton, scattered proton and  $J/\psi$  meson, respectively, are defined as follows:

- $Q^2 = -q^2 = -(k-k')^2$ , the negative four-momentum squared of the exchanged photon;
- $W^2 = (q + P)^2$ , the squared centre-of-mass energy of the photon-proton system;
- $y = (P \cdot q)/(P \cdot k)$ , the fraction of the positron energy transferred to the photon in the rest frame of the initial-state proton;
- $t = (P - P')^2 = (q - v)^2$ , the square of the four-momentum transfer at the proton vertex.

The following angles are used to describe the decay of the  $J/\psi$ :

- $\theta_h$  and  $\phi_h$ , the polar and azimuthal angles of the positively charged decay lepton in the helicity frame, defined as the  $J/\psi$  rest frame with the quantisation axis taken to be the  $J/\psi$  direction in the photon-proton centre-of-mass system. The origin of the azimuthal angle,  $\phi_h$ , corresponds to the case when the decay particles are produced in the production plane, defined as the plane containing the incident photon (assumed to be in the positron direction) and the  $J/\psi$  momentum vectors.

In addition to the above quantities,  $M_Y$ , the mass of the diffractively produced state  $Y$ , characterises the major background process, the proton-dissociative reaction  $ep \rightarrow eJ/\psi Y$ .

For the selected events,  $Q^2$  ranged from the kinematic minimum,  $Q_{min}^2 = M_e^2 y^2 / (1 - y) \approx 10^{-12} \text{ GeV}^2$ , where  $M_e$  is the positron mass, up to  $Q_{max}^2 \approx 1 \text{ GeV}^2$ , the value at which the scattered positron starts to be observed in the CAL, with a median  $Q^2$  of approximately  $5 \cdot 10^{-5} \text{ GeV}^2$ . Since the typical  $Q^2$  is small, it can be neglected in the reconstruction of the other kinematic variables.

The photon-proton centre-of-mass energy,  $W$ , can be expressed as  $W^2 \approx 2E_p(E - p_Z)_u$ , where  $E_p$  is the laboratory energy of the incoming proton and  $(E - p_Z)_u$  is the difference between the energy and the longitudinal momentum of the dilepton system.

The squared four-momentum transfer at the proton vertex is given by  $t \approx -p_T^2$ , the transverse-momentum squared of the dilepton system. Non-zero values of  $Q^2$  give  $t$  values that differ from  $-p_T^2$  by less than  $Q^2$ ; this effect is corrected for using the Monte Carlo simulation.

Since neither the scattered positron nor the scattered proton was observed, the kinematic variables were reconstructed using only the measured momenta of the decay particles. At low  $W$ , the  $J/\psi$  mesons are produced in the forward direction, while at high  $W$  they are produced in the backward direction. For the  $J/\psi \rightarrow \mu^+\mu^-$  sample, the CTD, FTD and FMUON information were used when available. For the  $J/\psi \rightarrow e^+e^-$  sample, the CTD or the CAL/SRTD information was used. The relevant *in situ* electron-energy resolution of the CAL for energies in the range  $3 < E < 20$  GeV averages  $\sigma(E)/E = 0.27/\sqrt{E}$  for this analysis [25].

## 4 Trigger and event selection

The events were selected online via a three-level trigger system [17]. The signature for exclusive  $J/\psi$  photoproduction events consists of a pair of charged leptons, with no other significant activity in either the CTD or the CAL, since the scattered positron and proton escape undetected down the beampipe at small scattering angles. For the two decay channels, the elasticity cuts described below were imposed. They restrict the photon virtuality to  $Q^2 \lesssim 1 \text{ GeV}^2$  and the mass of the dissociative system to  $M_Y \lesssim 3.0 \text{ GeV}$ . No cut on  $t$  was applied on either channel. To select candidate events for the muon and electron decay channels, different selection cuts were applied.

### 4.1 Muon channel

The trigger selected events with at least two tracks in the CTD or one track in the CTD and one track in FMUON. At least one track had to point towards an energy deposit compatible with a minimum ionising particle (m.i.p.) in the CAL and either a hit in the FMUI or a segment in the B/RMUI. The trigger efficiency for events that passed the offline selection cuts, defined below, was determined from independent triggers and from MC simulations to be between 50% and 75%, depending on  $W$ .

Events having the following characteristics were selected offline:

- exactly two oppositely charged tracks from a common vertex, with  $Z$ -coordinate  $|Z_{vertex}| < 50$  cm, at least one of which matches either a hit in the FMUI or a segment in the B/RMUI;
- each CTD track passes through at least three superlayers, effectively limiting the polar-angle region of these “CTD tracks” to  $17^\circ \leq \theta \leq 163^\circ$ ;
- the angle between the two tracks is less than  $174.2^\circ$ , in order to reject cosmic-ray events;

- CAL energy associated with each track consistent with the energy deposit of a m.i.p., i.e. between 0.8 and 5 GeV, with a ratio of at least 0.8 between the energies in the HAC and the EMC sections. The energy was associated with the track if it was inside a cone of radius 30 cm (in EMC) or 50 cm (in HAC), centred at the impact position of the track extrapolated on to the CAL;
- no CAL cell, apart from those associated with a candidate muon, with energy above the threshold level of 150 MeV to 200 MeV, depending on the calorimeter part and section. This elasticity requirement rejects proton-dissociative and inelastic events as well as deep inelastic scattering (DIS) events. The PRT1 was not used to veto the events.

To define the kinematic region in which both decay muons could be well reconstructed, the analysis was limited to the range  $20 < W < 170$  GeV. The requirement that CTD tracks traverse at least three superlayers leads to a small acceptance for two such tracks in the region  $20 < W < 30$  GeV. In this region, therefore, additional events were accepted with one CTD track and a second track in the FMUON spectrometer, which both measures the momentum and triggers the event. The FMUON track was re-fitted to the vertex including the FTD segments to improve the reconstruction parameters. In the kinematic region  $30 < W < 170$  GeV, only events with two CTD tracks were used.

## 4.2 Electron channel

The  $J/\psi \rightarrow e^+e^-$  events were selected online using two different trigger algorithms:

- the first algorithm was optimised for events with one or two tracks in the CTD. It required at least one track, but fewer than five tracks, in the CTD, a total energy deposit greater than 1.8 GeV in an EMC section of the CAL and an energy of less than 3.75 GeV in the region of  $60 \times 60$  cm<sup>2</sup> of FCAL around the forward beam pipe;
- the second algorithm was optimised for events with zero tracks in the CTD. It required at least two deposits in the RCAL EMC, each with an energy greater than 2.1 GeV.

The trigger efficiency for events that passed the offline selection cuts, defined below, was determined from independent triggers and from MC simulations to be between 80% and 90%, depending on  $W$ .

The following offline selection requirements were applied:

- for events with a reconstructed tracking vertex, the cut  $|Z_{VTX}| < 50$  cm was applied. Events without a vertex were accepted and were assigned a vertex  $Z$  position corresponding to the nominal interaction point;

- the CAL energy deposits were grouped into clusters. Events were selected for further analysis if they satisfied one of the following criteria:
  - for events with two CTD tracks, the CAL energy associated with each track, inside a cone of radius 25 cm centred at the impact position of the track extrapolated on to the CAL, had to be consistent with the energy deposition expected for an electron:  $E_{EMC}/E > 0.9$ , where  $E$  and  $E_{EMC}$  are, respectively, the total energy and the energy deposited in the EMC section. These two tracks were then considered electron candidates;
  - for events with one CTD track and one cluster not associated with it, the CAL energy associated with the track had to have  $E_{EMC}/E > 0.9$  and the CAL energy of the unassociated cluster had to be more than 3 GeV, with  $E_{EMC}/E > 0.98$ , to be considered an electron candidate;
  - for events with no CTD track, two clusters, each with CAL energy more than 3.5 GeV and with  $E_{EMC}/E > 0.98$ , were required as candidate electrons;
- any energy deposit in the CAL cells, not associated with either of the two electron candidates, was required to be less than either 200 MeV or 300 MeV, depending on the calorimeter part and section. This requirement<sup>3</sup> rejects proton-dissociative and inelastic events, as well as DIS events;
- further to reduce events from proton dissociation, the energy measured in the FPC was required to be less than 1 GeV.

The analysis was restricted to the kinematic region  $20 < W < 290$  GeV because the acceptance drops at lower  $W$  and the QED-Compton background dominates at higher  $W$ .

## 5 Monte Carlo simulation

The acceptance and the effects of the detector response were determined using samples of Monte Carlo (MC) events. The ZEUS detector response to the generated particles was simulated in detail using a program based on GEANT3.13 [26]. All the generated events were processed through the same reconstruction and analysis chain as the data.

The exclusive processes  $ep \rightarrow eJ/\psi p$  and  $ep \rightarrow e\psi(2S)p$  were modelled using the MC generators DIPSI [1, 27] and ZEUSVM [28]. The events were weighted with a  $\gamma p$  cross section proportional to  $W^\delta$  and with an exponential  $t$  dependence  $e^{bt}$ . The weight

---

<sup>3</sup> This elasticity requirement is less stringent than the one used for the selection of the muon sample because of an increased noise level in the CAL during the data taking in 1999 and 2000.

parameters,  $\delta = 0.70$  and  $b = 4.3 \text{ GeV}^{-2}$ , were chosen so as to describe the  $W$  and  $t$  dependence of the data, as discussed in Sections 9 and 10. The decay of the  $J/\psi$  mesons in the centre-of-mass system was generated with a  $(1 + \cos^2 \theta_h)$  distribution, consistent with the measurement presented in Section 8. The effect of the initial-state radiation on the acceptance, estimated using HERACLES 4.6.1 [29, 30], was 5% in the region  $20 < W < 30 \text{ GeV}$  and negligible at larger  $W$ . The final-state radiation of hard photons at large angles with respect to either of the two decay leptons decreases the acceptance, as these events are rejected by the elasticity requirements applied offline. The effect was estimated using PHOTOS [30, 31] and was found to be 1.3% in the muon analysis and up to 8% in the electron analysis. The acceptances,  $\mathcal{A}$ , corrected for these effects, are given in Table 1. They were calculated as the number of events reconstructed in a bin divided by the number of events generated in the same bin.

Proton-dissociative events,  $ep \rightarrow eJ/\psi Y$ , were modelled using the generator EPSOFT [32], which simulates  $\gamma p$  interactions assuming the exchange of the soft-Pomeron trajectory. At fixed  $W$  and  $t$ , it models the mass spectrum of the baryon system  $Y$  according to  $d\sigma/dM_Y^2 \propto M_Y^{-\beta}$ , with  $M_Y > 1.25 \text{ GeV}$ . The multiplicity distribution of hadrons from the decay of the proton-dissociative system and their transverse momenta with respect to the proton-Pomeron collisions axis are simulated to describe the ZEUS photoproduction data and hadron-hadron single-diffractive results. The longitudinal momenta are generated using a uniform distribution in rapidity. The simulation parameters  $\delta = 0.70$ ,  $b = 0.65 \text{ GeV}^{-2}$  and  $\beta = 2.6$  were chosen to describe the  $W$ ,  $t$  and  $M_Y$  dependence of the data, as discussed in Section 6.3. For the region  $M_Y < 2 \text{ GeV}$ ,  $b = 4.0 \text{ GeV}^{-2}$  was used. This reflects the steeper  $t$  distribution observed in low-mass hadron-hadron diffraction [33, 34].

The QED  $\gamma\gamma \rightarrow l^+l^-$  background was simulated using the LPAIR [35] generator. The QED-Compton scattering,  $ep \rightarrow e\gamma p$ , background was simulated using the COMPTON2 [36] generator.

## 6 Mass spectra and background subtraction

The invariant-mass spectra for the muon- and electron-pair candidates, after all offline cuts, are shown in Figs. 1 and 2 for representative  $W$  bins. The mass resolution is excellent in the region  $30 < W < 150 \text{ GeV}$ , where both reconstructed leptons pass through all CTD layers, and decreases at lower and higher  $W$  values, where the leptons are produced in the forward and rear direction, respectively, at the edges of the CTD acceptance. In the analysis of the electron decay channel, the kinematic region was extended at very high  $W$  by reconstructing the electrons in the RCAL and SRTD. The mass spectra of the electron



pairs have a tail at low mass due to photon bremsstrahlung.

The final samples contain backgrounds from non-resonant sources: QED  $\gamma\gamma$  processes, QED-Compton scattering and other non-resonant background (dominated by misidentified pion production), as well as from resonant processes: diffractive  $\psi(2S)$  production and proton dissociation. Contamination from non-diffractive  $J/\psi$  production,  $ep \rightarrow eJ/\psi X$ , estimated using the MC generator HERWIG 5.8 [37], is negligible.

## 6.1 Non-resonant background

Background from the QED process  $\gamma\gamma \rightarrow l^+l^-$ , in which a lepton pair is produced by the fusion of a photon radiated by the positron with a photon radiated by the proton, was estimated using the LPAIR MC normalised to the data in the mass region outside the  $J/\psi$  and  $\psi(2S)$  resonances. It is shown in the dilepton-mass spectra of Figs. 1 and 2. The typical contribution in the signal region is 10% for the muon sample and up to 20% for the electron sample.

Pions produced at low angles in the forward direction can be misidentified as muons or electrons. This background dominates at low masses and for  $W < 50$  GeV, as can be seen in Figs. 1(a) and 2(a,b).

For the electron sample, there is an additional contribution from QED-Compton scattering with initial-state radiation. It was estimated using the COMPTON2 MC normalised to the data in the mass region outside the resonances for  $W > 230$  GeV, where it dominates the background distribution, as shown in Fig. 2. The size of this background ranges from 3% at  $W = 200$  GeV to 50% at  $W = 275$  GeV. The total non-resonant contributions are given in Table 1.

## 6.2 Events from $\psi(2S)$ production

Events from  $\psi(2S)$  production can fake exclusive  $J/\psi$  events, mainly through the decay  $\psi(2S) \rightarrow J/\psi + \text{neutrals}$ , with a branching ratio  $\mathcal{B} = (23.1 \pm 2.3)\%$  [38], when the  $J/\psi$  decays into two leptons and the neutral particles are not detected in the CAL. An additional source of background comes directly from  $\psi(2S) \rightarrow l^+l^-$  decays, with a branching ratio  $\mathcal{B} = (1.03 \pm 0.35)\%$  [38], since the mass window used to count the  $J/\psi$  signal, for  $W \lesssim 35$  GeV and  $W \gtrsim 140$  GeV, is large enough to include the  $\psi(2S)$  mass at 3.685 GeV. The number of events from  $\psi(2S)$  production present in the  $J/\psi$  elastic sample was estimated using the  $\psi(2S)$  DIPSI MC events and the ratio of production cross sections,  $\psi(2S)/(J/\psi) = 0.150 \pm 0.027(\text{stat.}) \pm 0.022(\text{syst.})$  [39], to be smaller than 7%, as shown in Table 1.

### 6.3 Proton dissociation

The largest source of background is given by the diffractive production of  $J/\psi$  mesons with proton dissociation,  $ep \rightarrow eJ/\psi Y$ , when the system  $Y$  has a small mass and its decay products are not detected in either the FCAL, the PRT1 or the FPC.

To estimate this background, the elasticity cut was removed in the region of fragmentation of the system  $Y$ ; the proton-dissociative data obtained in this way were used to tune the EPSOFT MC generator. The data and the fraction of MC events in which energy was deposited in the PRT1 or the FPC were then used to estimate the number of proton-dissociative events contaminating the exclusive  $J/\psi$  sample.

The parameters  $b$  and  $\beta$  of the EPSOFT MC generator were tuned using a sample of dimuon events triggered by the B/RMUI. These data were selected as described in Section 4.1 but, for those FCAL cells with  $\theta < 30^\circ$ , the elasticity requirement was removed and an energy of at least 300 MeV in both EMC and HAC sections was required. A rapidity gap of at least  $\Delta\eta > 1.3$  between the  $J/\psi$  meson and the products of the proton-dissociative system was required. The final sample of  $J/\psi$  candidates, in the kinematic region  $90 < W < 130$  GeV, consisted of about 600 events. The data sample corresponds, according to MC simulations, to the region  $3.5 < M_Y < 30$  GeV and  $p_T^2 < 10$  GeV<sup>2</sup>. The  $b$  slope and  $\beta$  parameters were determined to be  $0.65 \pm 0.10$  GeV<sup>-2</sup> and  $2.6 \pm 0.3$ , respectively, from the study of the  $p_T^2$  and visible CAL-energy distributions. The  $W$  distribution for the proton-dissociative process was consistent with that of the exclusive channel. A similar study performed for the electron-decay channel, using a smaller sample of data triggered without the veto on energy deposited in the FCAL region around the beam pipe, yielded values of  $b$  and  $\beta$  consistent with those determined from the muon sample.

The proton-dissociative events misidentified as exclusive  $J/\psi$  production were subtracted in each  $(W, t)$  bin for the cross sections presented here, for both the muon and the electron analyses.

In the muon analysis, the contribution from proton-dissociative events in the elastic sample was estimated using the PRT1. In each  $W$  and  $t$  bin, the quantity  $f_{p-diss} = f_{PRT1}^{data} \cdot \frac{1}{\epsilon}$ , was computed, where  $f_{PRT1}^{data}$  is the fraction of the data tagged in the PRT1 and  $\epsilon$  is the MC tagging efficiency, defined as the probability to obtain a tag in PRT1 in EPSOFT events. Using  $f_{PRT1}^{data} = 12.6\%$  and  $\epsilon = 57.2\%$ ,  $f_{p-diss}$  was estimated to be  $(22.0 \pm 2.0(stat.) \pm 2.0(syst.))\%$  for  $|t| < 2$  GeV<sup>2</sup>, with no  $W$  dependence. The fraction of  $f_{p-diss}$  was estimated to increase with  $t$  from  $(11.0^{+3.1}_{-1.4}(stat. + syst.))\%$ , in the first  $t$  bin, up to  $(49^{+14}_{-6}(stat. + syst.))\%$ , for  $1.2 < |t| < 1.8$  GeV<sup>2</sup>.

In 1998, the PRT1 was no longer used. The FPC was inserted and was used to veto proton-dissociative events. In the electron analysis, which uses the data taken in 1999 and 2000, the amount of proton-dissociative background in the elastic sample was estimated from

$f_{p-diss} = f_{FPC}^{data} \cdot (\frac{1}{\epsilon} - 1)$  and found to be  $(17.5 \pm 1.3(stat.)_{-3.2}^{+3.7}(syst.))\%$ , using  $f_{FPC}^{data} = 12\%$  for the FPC-tagged events and  $\epsilon = 40.7\%$ , where  $\epsilon$  is defined as the probability to obtain a tag in FPC in EPSOFT events. The formula is different with respect to the muon case because the events tagged by the FPC were also rejected. The fraction of  $f_{p-diss}$  was estimated to increase with  $t$  from  $(6_{-4}^{+3}(stat. + syst.))\%$  at low  $t$  to  $(28_{-5}^{+8}(stat. + syst.))\%$  at  $0.85 < t < 1.15 \text{ GeV}^2$ .

As an independent check on the estimation of the proton-dissociative background, an alternative model to EPSOFT was used. In the baryon resonance region, at low  $M_Y$ , a resonant component with slope  $b = 6.5 \text{ GeV}^{-2}$  was considered. A second component due to non-resonant proton dissociation with slope  $b = 0.65 \text{ GeV}^{-2}$  was added. The two components were constrained to satisfy the first moment of the finite-mass sum rule [40]. This model yielded results that agreed with those from EPSOFT to within 2% for both the cross section and the  $b$  slope.

## 6.4 Signal determination

Since the mass spectra have shapes and background contributions that vary with  $W$ ,  $t$  and the decay channel, different procedures were used in the muon and electron analyses to determine the number of signal events.

For the muon analysis, the signal events were counted in a mass window corresponding to  $\pm$  three standard deviations of the Gaussian fit from the mean fitted value of the  $J/\psi$  mass. Since the mass resolution depends on the kinematic region, the mass windows were different for different  $W$  and  $t$  bins. The number of  $\gamma\gamma \rightarrow \mu^+\mu^-$  background events was estimated as described in Section 6.1 and subtracted in each mass window to obtain the number of  $J/\psi$  candidate events. For the lowest  $W$  bin, there is a remaining background, coming from misidentified pions. The mass spectrum was then fitted to the sum of the distribution predicted by the signal MC and a single exponential function for the background.

For the electron analysis, the backgrounds due to QED-Compton scattering and from  $\gamma\gamma \rightarrow e^+e^-$  were subtracted. The remaining mass spectrum was then fitted, in each bin, to the sum of the distribution predicted by the signal MC and a single exponential function for the remaining background. The latter is dominated by misidentified pions. The MC gives a good description of the  $M_{e^+e^-}$  distributions observed in the data with typical  $\chi^2/\text{ndf}$  better than 1.5

## 7 Systematic uncertainties

The systematic uncertainties on the cross sections are given separately for the two decay channels. For the muon channel, the following sources of uncertainty were considered.

- trigger efficiency: the uncertainty due to that of the trigger efficiency was  $\pm 5\%$  for the CTD track reconstruction and up to  $\pm 7\%$  for the muon selection;
- event selection: the minimum number of required CTD superlayers was raised from three to four; the cut on the angle between two tracks was relaxed from  $174.2^\circ$  to  $176.4^\circ$ ; the criteria for the identification of a m.i.p. in the CAL were varied and the cell energy threshold for the selection of exclusive events was increased from 150 or 200 MeV to 300 MeV. The resulting uncertainty was  $\pm 3\%$ . For events in the range  $20 < W < 30$  GeV, the uncertainty due to the track reconstruction in the FMUON/FTD was  $\pm 11\%$ ;
- MC model dependence: the uncertainty was estimated by varying the parameters  $b$  and  $\delta$  of the DIPSI MC simulation within the range  $4.1 < b < 4.5 \text{ GeV}^{-2}$  and  $0.60 < \delta < 0.75$ . The centre-of-mass decay angular distribution of the muons was changed to  $[1 + \alpha + (1 - 3\alpha) \cos^2 \theta_h]$  with  $\alpha = -0.05$ , consistent with the measurement presented in Section 8. The overall uncertainty due to model dependence was  $\pm 5\%$ ;
- proton-dissociative subtraction: the uncertainty on the modelling of the hadronic final state in proton-dissociative events was estimated to be  $\pm 2\%$  by varying the parameters of the simulation by  $\pm 0.3$  for  $\beta$  and  $\pm 0.10 \text{ GeV}^{-2}$  ( $\pm 2 \text{ GeV}^{-2}$ ) for  $b$  when  $M_Y > 2 \text{ GeV}$  ( $M_Y < 2 \text{ GeV}$ ), as discussed in Section 6;
- non-resonant background subtraction: the uncertainty was typically  $\pm 2\%$ . In the lowest  $W$  bin, the uncertainty was  $7\%$ , as determined by the fit; ;
- the uncertainty in the luminosity determination was  $\pm 1.7\%$  for the 1996-1997 running period.

For the electron channel, the following sources of uncertainty were considered:

- trigger efficiency: the estimated uncertainty was  $\pm 2.5\%$  for the CTD,  $\pm(1 - 5)\%$ , depending on  $W$ , for the CAL energy threshold and  $\pm 3\%$  for the trigger stream requiring two isolated electromagnetic clusters;
- event selection: the effect of varying the elasticity requirements by raising the threshold by 100 MeV was  $-2.5\%$  to  $+2.5\%$ , depending on  $W$ ;
- MC model dependence: the uncertainty, estimated in the same way as described for the muon channel, was less than  $\pm 2.5\%$ ;
- proton-dissociative subtraction: the uncertainty, estimated as described for the muon channel, was  ${}_{-3.5}^{+4.0}\%$ ;

- non-resonant background subtraction: the uncertainty in the normalisation of this background, as determined by the fit, varied between 1 and 6%, depending on  $W$ ;
- the uncertainty in the luminosity determination was  $\pm 2.25\%$  in the years 1999 and 2000.

The overall systematic uncertainty was determined by adding the uncertainties in quadrature. An additional uncertainty of 1.7% [38] associated with the branching ratio  $\mathcal{B}_{J/\psi \rightarrow l+l^-}$  was not included. Since the major sources of systematic uncertainty are mostly independent of  $W$ , they have a small influence on the determination of  $\delta$  and the Pomeron trajectory.

## 8 Decay angular distributions

Since the decay angular distributions were used to reweight the MC simulated events and thus affect the cross-section measurements, they are discussed first. They were used to investigate the helicity structure of  $J/\psi$  production. The decay angular distribution is a function of  $\theta_h$  and  $\phi_h$ , the polar and azimuthal angles of the positively charged lepton in the helicity frame. The normalised angular distributions can be expressed [41] in the form

$$\frac{1}{N} \frac{dN}{d \cos \theta_h} = \frac{3}{8} [1 + r_{00}^{04} + (1 - 3r_{00}^{04}) \cos^2 \theta_h] \quad (3)$$

and

$$\frac{1}{N} \frac{dN}{d \phi_h} = \frac{1}{2\pi} [1 + r_{1-1}^{04} \cos 2\phi_h], \quad (4)$$

where the  $J/\psi$  spin-density matrix element  $r_{00}^{04}$  represents the probability that the produced  $J/\psi$  has helicity 0 and  $r_{1-1}^{04}$  is related to the interference between the non-flip and double-flip amplitudes. If the  $J/\psi$  retains the helicity of the almost-real photon, as in the hypothesis of  $s$ -channel helicity conservation (SCHC),  $r_{00}^{04}$  and  $r_{1-1}^{04}$  should both be approximately zero.

The angular distributions of the leptons from  $J/\psi$  decay are presented in Fig. 3. They were measured in the kinematic range  $30 < W < 170$  GeV and  $|t| < 1$  GeV<sup>2</sup>, using events in which both leptons were measured in the CTD. The non-resonant background was subtracted in each angular bin. No subtraction of the dissociative contribution was made, since the proton-dissociative sample, discussed in Section 6.3, displayed similar angular distributions to the elastic events. The  $\psi(2S)$  events were assumed to have the same angular distribution as the  $J/\psi$  events and were not subtracted.

The elements  $r_{00}^{04}$  and  $r_{1-1}^{04}$ , obtained by fitting the acceptance-corrected  $\theta_h$  and  $\phi_h$  distributions to Eqs. (3) and (4), are

$$r_{00}^{04} = -0.017 \pm 0.015(stat.) \pm 0.009(syst.)$$

and

$$r_{1-1}^{04} = -0.027 \pm 0.013(stat.) \pm 0.005(syst.).$$

Thus, to within two standard deviations, the SCHC hypothesis holds, as expected for heavy mesons [42].

## 9 $W$ dependence of the cross section

The  $\gamma p$  cross section for exclusive  $J/\psi$  production was evaluated from the  $ep$  cross section using the expression

$$\sigma_{\gamma p \rightarrow J/\psi p} = \frac{\sigma_{ep \rightarrow e J/\psi p}}{\Phi} = \frac{1}{\Phi} \cdot \frac{(N_{obs} - N_{non-res} - N_{\psi(2S)}) \cdot (1 - f_{p-diss})}{\mathcal{L} \cdot \mathcal{A} \cdot \mathcal{B}}, \quad (5)$$

where  $\Phi$  is the effective photon flux [43],  $N_{obs}$  is the number of events in the signal mass region,  $N_{non-res}$  is the number of non-resonant background events,  $N_{\psi(2S)}$  is the number of events from  $\psi(2S)$  production,  $f_{p-diss}$  is the fraction of proton-dissociative events,  $\mathcal{L}$  is the integrated luminosity,  $\mathcal{A}$  is the acceptance and  $\mathcal{B}$  is the branching ratio, where  $\mathcal{B} = (5.93 \pm 0.10)\%$  for the electron channel and  $(5.88 \pm 0.10)\%$  for the muon channel [38].

The numbers of events, the acceptance, the flux factors and the cross sections are given in  $W$  bins for each decay mode in Table 1. The cross section is shown as a function of  $W$  in Fig. 4. No cut on  $t$  was applied. The small difference ( $\sim 4\%$ ) in the normalisation of the muon and the electron values is within the correlated uncertainty associated with each decay channel. The values are larger than those determined previously by ZEUS [14]. The differences are due to a better understanding of the acceptance and trigger efficiency and of the background subtraction. Because of these improvements, the results of this paper supersede those of the previous publication.

Results from the H1 Collaboration [15] and from fixed-target experiments [44, 45] are also displayed in Fig. 4. While the  $W$  dependence is similar, there is a normalisation difference between the H1 and ZEUS values.

The results of fits of the form  $\sigma \propto (W/90 \text{ GeV})^\delta$  to the muon data and, separately, to the electron data are given in Table 2. A common fit to the data with  $W > 30 \text{ GeV}$ , including both the muon and the electron measurements, with statistical and systematic

uncertainties added in quadrature, yields a value of  $\delta = 0.69 \pm 0.02(stat.) \pm 0.03(syst.)$ . This result, shown as the curve in Fig. 4, confirms the strong energy dependence of the cross section observed previously [14, 15]. The measurements for  $W < 30$  GeV were not included in this fit to avoid possible effects due to the charm production threshold [46]. However, the result of a fit including the points with  $W < 30$  GeV does not significantly change the fitted value of  $\delta$ .

The ZEUS data are compared in Fig. 5 to leading-log-approximation (LLA) pQCD calculations [5], based on open  $c\bar{c}$  production and parton-hadron duality, using the CTEQ5M [47] (dashed curve) or MRST99 [48] (dotted curve) parton-density functions (PDF). The gluon density is evolved using “skewed” evolution equations [49].

The solid curve in Fig. 5 is the result of a LLA pQCD calculation [6] based on the interaction of the proton with  $q\bar{q}$  dipoles with small transverse size via two-gluon exchange. The model uses the CTEQ4L gluon PDF [50] evolved using skewed evolution. This calculation is sensitive to the value of  $\lambda$ , a scaling parameter that relates the transverse size of the dipole to the four-momentum scales in the interaction cross section. The curve shown uses  $\lambda = 4$ , which gives a dependence on  $W$  that is less steep than for  $\lambda = 10$ , which was favoured by studies of the proton structure function,  $F_2$ .

These predictions qualitatively describe the steep rise of the cross section with energy. At  $W = 250$  GeV, the gluon density is being probed in these models [6] at  $x \sim 10^{-4}$ , outside the range in which it is well constrained by global PDF analyses; the results are, therefore, sensitive to the PDF used. However, no discrimination between the gluon PDF can be made from the curves shown in Fig. 5 due to the large theoretical uncertainties from higher-twist contributions and the QCD scales due to missing higher-order terms. In addition, skewed parton distributions [51] are, as yet, relatively poorly constrained since the proton structure function  $F_2$  is not very sensitive to them.

Also shown in Fig. 5 is the result (dot-dashed curve) of a calculation [52] based on a dipole model [53]. The  $J/\psi$  wave-function was assumed to be Gaussian in both the transverse and longitudinal momenta of the quarks. The normalisation was fixed from the  $b_0$  value reported in the next section. The  $W$  dependence of the model is in reasonable agreement with the present data.

## 10 Differential cross-section $d\sigma/dt$ and the Pomeron trajectory

The differential cross-section  $d\sigma_{\gamma p \rightarrow J/\psi p}/dt$  was calculated, in bins of  $W$ , separately for the muon and electron  $J/\psi$  decay channels in the kinematic range  $-t < 1.8 \text{ GeV}^2$  and

$-t < 1.25 \text{ GeV}^2$ , respectively. The results are shown in Fig. 6 for four representative ranges of  $W$ . In each  $W$  bin, a fit of the form  $d\sigma/dt = d\sigma/dt|_{t=0} \cdot e^{bt}$  was performed. For the muon sample, the fit was performed in the restricted range  $-t < 1.2 \text{ GeV}^2$ , where the uncertainty resulting from the subtraction of proton-dissociative events is small. The results of the fits are given in Table 1. The muon and electron analyses give consistent results for  $d\sigma/dt|_{t=0}$  and  $b$ , as shown in Figs. 6 and 7.

The  $b$  slope increases with  $W$  and, in the geometrical picture of the interaction, is approximately equal to that expected from the size of the proton [33], which suggests that the size of the  $J/\psi$  is small compared to that of the proton.

A value of  $\alpha'_{IP}$  was obtained by fitting the  $W$  dependence of  $b$  to the function  $b(W) = b_0 + 4\alpha'_{IP} \cdot \ln(W/90 \text{ GeV})$ , according to Eq. (2). The results for both the muon and electron analyses, given in Table 2, are in good agreement. The systematic uncertainties were estimated by repeating the fit for each uncertainty not correlated in  $W$  and adding the deviations from the nominal value in quadrature. The result of the combined measurement, shown as the line in Fig. 7, is

$$b_0 = 4.15 \pm 0.05(stat.)_{-0.18}^{+0.30}(syst.) \text{ GeV}^{-2}$$

$$\alpha'_{IP} = 0.116 \pm 0.026(stat.)_{-0.025}^{+0.010}(syst.) \text{ GeV}^{-2}.$$

The systematic uncertainties were computed from the combination of the muon and electron analyses, taking into account the common systematic uncertainties.

The Pomeron trajectory was determined directly by measuring the variation of the  $W$  dependence of the elastic cross section at fixed  $t$ , as parameterised in Eq. (1). This method is insensitive to the proton-dissociative background, since the latter was measured to be independent of  $W$ , as described in Section 6. In Fig. 8, the measurements of  $d\sigma/dt$  used in this determination of  $\alpha_{IP}(t)$  are presented as a function of  $W$  for fixed  $t$ ; the line in each plot is the result of a fit of the form  $d\sigma/dt \propto W^{4[\alpha_{IP}(t)-1]}$ . The resulting values of  $\alpha_{IP}(t)$ , given in Table 3, are shown in Fig. 9, with the published H1 results [15], as a function of  $t$ . They were fitted to the linear form  $\alpha_{IP}(t) = \alpha_{IP}(0) + \alpha'_{IP}t$ . The separate fits from the muon and electron analyses are given in Table 2 and are in good agreement. The combined measurement gives

$$\alpha_{IP}(0) = 1.200 \pm 0.009(stat.)_{-0.010}^{+0.004}(syst.)$$

and

$$\alpha'_{IP} = 0.115 \pm 0.018(stat.)_{-0.015}^{+0.008}(syst.) \text{ GeV}^{-2}.$$

The systematic uncertainties were computed from the combination of the muon and electron analyses, taking into account the common systematic uncertainties. The result of



the fit was stable with respect to changes in the  $t$  range used for the fit. The slope,  $\alpha'_{\mathbb{P}}$ , measured with the present data, is not consistent with zero and therefore indicates a small shrinkage. The increase with  $W$  of the cross section and of the  $b$  slope, parameterised by  $\alpha_{\mathbb{P}}(0)$  and  $\alpha'_{\mathbb{P}}$ , respectively, are in agreement with pQCD-based models [6, 54]. The values of  $\alpha_{\mathbb{P}}(0)$  and  $\delta$  are compatible, after taking account of the measured value of  $\alpha'_{\mathbb{P}}$ . The soft-Pomeron trajectory  $\alpha_{\mathbb{P}} = 1.08 + 0.25 \cdot t$  [11, 55] is inconsistent with the present data. However, the contribution of the soft Pomeron plus a hard Pomeron as proposed by Donnachie and Landshoff [56] may well be able to describe the data.

## 11 Conclusions

The exclusive photoproduction of  $J/\psi$  mesons has been studied at HERA with the ZEUS detector in the kinematic range  $20 < W < 290$  GeV using both the muon and the electron decay channels. The  $J/\psi$  spin-density matrix elements,  $r_{00}^{04}$  and  $r_{1-1}^{04}$ , have been measured; their values are consistent, within two standard deviations, with the hypothesis of  $s$ -channel helicity conservation.

The  $\gamma p \rightarrow J/\psi p$  cross section exhibits a strong dependence on  $W$ , which can be parameterised by a power-like dependence of the type  $W^\delta$ , with  $\delta = 0.69 \pm 0.02(stat.) \pm 0.03(syst.)$ . This behaviour is described by pQCD-based models and can be understood as due to the increase of the gluon density in the proton for decreasing values of the parton fractional momentum.

The differential cross-section  $d\sigma_{\gamma p \rightarrow J/\psi p}/dt$  has been measured as a function of  $W$  for  $|t| < 1.8$  GeV<sup>2</sup>. It can be described by an exponential function in  $t$ , with a slope  $b = 4.15 \pm 0.05(stat.)_{-0.18}^{+0.30}(syst.)$  GeV<sup>-2</sup> at  $W = 90$  GeV, which increases logarithmically with  $W$ .

The parameters of the Pomeron trajectory,  $\alpha_{\mathbb{P}}(0)$  and  $\alpha'_{\mathbb{P}}$ , have been determined from the  $W$  and  $t$  dependence of  $d\sigma_{\gamma p \rightarrow J/\psi p}/dt$ . The intercept is  $\alpha_{\mathbb{P}}(0) = 1.200 \pm 0.009(stat.)_{-0.010}^{+0.004}(syst.)$  and the slope is  $\alpha'_{\mathbb{P}} = 0.115 \pm 0.018(stat.)_{-0.015}^{+0.008}(syst.)$  GeV<sup>-2</sup>. These values are inconsistent with those expected from the exchange of a soft Pomeron. The data indicate that  $\alpha'_{\mathbb{P}}$  is different from zero but smaller by a factor of two than the value measured in soft hadronic interactions.

Clearly therefore, the description of  $J/\psi$  production lies within the realm of perturbative QCD. A quantitative description comparable to the precision of the current data requires further theoretical progress.

## Acknowledgments

We thank the DESY directorate for their strong support and encouragement, and the HERA machine group for their diligent efforts. We are grateful for the support of the DESY computing and network services. The design, construction and installation of the ZEUS detector have been made possible by the ingenuity and effort of many people from DESY and home institutes who are not listed as authors. It is a pleasure to thank M. McDermott and T. Teubner for providing us with their model predictions and E. Levin for useful discussions.

## References

- [1] M.G. Ryskin, *Z. Phys.* **C 57**, 89 (1993);  
M.G. Ryskin et al., *Z. Phys.* **C 76**, 231 (1997).
- [2] S.J. Brodsky et al., *Phys. Rev.* **D 50**, 3134 (1994).
- [3] J. Bartels et al., *Phys. Lett.* **B 375**, 301 (1996).
- [4] I.F. Ginzburg and D.Yu. Ivanov, *Phys. Rev.* **D 54**, 5523 (1996).
- [5] A.D. Martin, M.G. Ryskin and T. Teubner, *Phys. Rev.* **D 62**, 14022 (2000).
- [6] L. Frankfurt, M. McDermott and M. Strikman, *JHEP* **103**, 45 (2001).
- [7] E. Gotsman et al., *Phys. Lett.* **B 503**, 277 (2001).
- [8] S. Munier, A.M. Stasto and A.H. Mueller, *Nucl. Phys.* **B 603**, 427 (2001).
- [9] J.P. Ma and Jia-Sheng Xu, Preprint hep-ph/0111391, 2001.
- [10] P.D.B. Collins, *An Introduction to Regge Theory and High Energy Physics*. Cambridge University Press, 1977.
- [11] G.A. Jaroszkiewicz and P.V. Landshoff, *Phys. Rev.* **D 10**, 170 (1974).
- [12] H. Abramowicz, L. Frankfurt and M. Strikman, *Surveys in High Energy Physics* **11**, 51 (1997).
- [13] N.N. Nikolaev, B.G. Zakharov and V.R. Zoller, *Phys. Lett.* **B 366**, 337 (1996).
- [14] ZEUS Coll., J. Breitweg et al., *Z. Phys.* **C 75**, 215 (1997).
- [15] H1 Coll., C. Adloff et al., *Phys. Lett.* **B 483**, 23 (2000).
- [16] A. Levy, *Phys. Lett.* **B 424**, 191 (1998).
- [17] ZEUS Coll., U. Holm (ed.), *The ZEUS Detector*. Status Report (unpublished), DESY, 1993, available on <http://www-zeus.desy.de/bluebook/bluebook.html>.
- [18] N. Harnew et al., *Nucl. Instr. and Meth.* **A 279**, 290 (1989);  
B. Foster et al., *Nucl. Phys. Proc. Suppl.* **B 32**, 181 (1993);  
B. Foster et al., *Nucl. Instr. and Meth.* **A 338**, 254 (1994).
- [19] M. Derrick et al., *Nucl. Instr. and Meth.* **A 309**, 77 (1991);  
A. Andresen et al., *Nucl. Instr. and Meth.* **A 309**, 101 (1991);  
A. Caldwell et al., *Nucl. Instr. and Meth.* **A 321**, 356 (1992);  
A. Bernstein et al., *Nucl. Instr. and Meth.* **A 336**, 23 (1993).
- [20] A. Bamberger et al., *Nucl. Instr. and Meth.* **A 450**, 235 (2000).
- [21] A. Bamberger et al., *Nucl. Instr. and Meth.* **A 401**, 63 (1997).

- [22] G. Abbiendi et al., Nucl. Instr. and Meth. **A 333**, 342 (1993).
- [23] ZEUS Collab., J. Breitweg et al., Z. Phys. **C 75**, 421 (1997).
- [24] J. Andruszkow et al., Acta Phys. Polon. **B 32**, 2025 (2001).
- [25] B. Mellado, *Measurement of Diffractive Heavy Vector Meson Photoproduction at HERA with the ZEUS detector*. Ph.D. Thesis, Columbia University, New York, USA, Report DESY-THESIS-2002-002, DESY, 2002.
- [26] R. Brun et al., GEANT3, Technical Report CERN-DD/EE/84-1, CERN, 1987.
- [27] M. Arneodo, L. Lamberti and M. Ryskin, Comp. Phys. Comm. **100**, 195 (1997).
- [28] K. Muchorowski, *Analysis of Exclusive  $\rho^0$  Production in Deep Inelastic ep Scattering at 300 GeV Centre-of-mass Energy (Experiment ZEUS at HERA Accelerator)*. Ph.D. Thesis, Warsaw University, Warsaw, Poland, 1996, (unpublished).
- [29] A. Kwiatkowski, H. Spiesberger and H.-J. Möhring, Comp. Phys. Comm. **69**, 155 (1992). Also in *Proc. Workshop on Physics at HERA*, 1991, DESY, Hamburg.
- [30] T. Abe, *Elastic Electroproduction of  $J/\psi$  at HERA*. Ph.D. Thesis, University of Tokyo, Tokyo, Japan, 2001, (unpublished).
- [31] E. Barberio and Z. Was, Comp. Phys. Comm. **79**, 291 (1994).
- [32] M. Kasprzak, *Inclusive Properties of Diffractive and Non-diffractive Photoproduction at HERA*. Ph.D. Thesis, Warsaw University, Warsaw, Poland, Report DESY F35D-96-16, DESY, 1996;  
L. Adamczyk, *Vector Meson Photoproduction at Large Momentum Transfer at HERA*. Ph.D. Thesis, University of Mining and Metallurgy, Cracow, Poland, Report DESY-THESIS-1999-045, DESY, 1999.
- [33] Y. Akimov et al., Phys. Rev. **D 14**, 3148 (1976).
- [34] M. Albrow et al., Nucl. Phys. **B 108**, 1 (1976).
- [35] J.A.M. Vermaseren, Nucl. Phys. **B 229**, 347 (1983).
- [36] T. Carli et al., in *Proc. Workshop on Physics at HERA*, eds. W. Buchmüller and G. Ingelman, Vol. 3, p. 1468. Hamburg, Germany, DESY, 1992.
- [37] G. Marchesini et al., Comp. Phys. Comm. **67**, 465 (1992).
- [38] Particle Data Group, D.E. Groom et al., Eur. Phys. J. **C 15**, 1 (2000).
- [39] H1 Coll., C. Adloff et al., Phys. Lett. **B 421**, 385 (1998).
- [40] G. Alberi and G. Goggi, Phys. Rev. **74**, 1 (1980).
- [41] K. Schilling and G. Wolf, Nucl. Phys. **B 61**, 381 (1973).
- [42] I.F. Ginzburg, S.L. Panfil and V.G. Serbo, Nucl. Phys. **B 296**, 569 (1988).

- [43] V.M. Budnev et al., Phys. Rep. **15**, 181 (1974).
- [44] E401 Coll., M. Binkley et al., Phys. Rev. Lett. **48**, 73 (1982).
- [45] E516 Coll., B.H. Denby et al., Phys. Rev. Lett. **52**, 795 (1984).
- [46] L.L. Jenkovszky, E.S. Martynov and F. Paccanoni, in *Proc. Int. Workshop High-energy Physics*, eds. G. Bugrij et al., p. 170. Kiev, 1996;  
R. Fiore, L.L. Jenkovszky and F. Paccanoni, Eur. Phys. J. **C 10**, 461 (1999).
- [47] CTEQ Coll., H.L. Lai et al., Eur. Phys. J. **C 12**, 375 (2000).
- [48] A.D. Martin et al., Eur. Phys. J. **C 4**, 463 (1998).
- [49] A. Freund and V. Guzey, Phys. Lett. **B 462**, 178 (1999);  
J. Bartels and M. Loewe, Z. Phys. **C 12**, 263 (1982).
- [50] H.L. Lai et al., Phys. Rev. **D 55**, 1280 (1997).
- [51] X.-D. Ji, J. Phys. **G 24**, 1181 (1998).
- [52] A.C. Caldwell and M.S. Soares, Nucl. Phys. **A 696**, 125 (2001).
- [53] K. Golec-Biernat and M. Wüsthoff, Phys. Rev. **D 59**, 014017 (1999);  
K. Golec-Biernat and M. Wüsthoff, Phys. Rev. **D 60**, 114023 (1999).
- [54] S.J. Brodsky et al., JETP Lett. **70**, 155 (1999).
- [55] A. Donnachie and P.V. Landshoff, Phys. Lett. **B 348**, 213 (1995).
- [56] A. Donnachie and P.V. Landshoff, Phys. Lett. **B 470**, 243 (1999).

$W$ (GeV)	Mode	$N_{obs}$	$N_{non-res}$	$N_{\psi(2S)}$	$\mathcal{A}$	$\Phi$	$\sigma$ (nb)	$\frac{d\sigma}{dt} _{t=0}$ (nb/GeV <sup>2</sup> )	$b$ (GeV <sup>-2</sup> )
20-30	$\mu^+\mu^-$	139	36	7	0.0314	0.04520	$32.6 \pm 5.4 \pm 5.2$		
30-50	$\mu^+\mu^-$	1883	207	12	0.260	0.05376	$41.5 \pm 1.1 \pm 3.3$	$152 \pm 7_{-9}^{+16}$	$3.93 \pm 0.12_{-0.14}^{+0.31}$
50-70	$\mu^+\mu^-$	1512	54	19	0.281	0.03195	$55.8 \pm 1.5 \pm 4.6$	$208 \pm 11_{-16}^{+24}$	$4.02 \pm 0.15_{-0.14}^{+0.26}$
70-90	$\mu^+\mu^-$	1299	62	16	0.294	0.02176	$66.6 \pm 2.0 \pm 7.0$	$276 \pm 15_{-29}^{+40}$	$4.27 \pm 0.15_{-0.15}^{+0.28}$
90-110	$\mu^+\mu^-$	1142	54	15	0.322	0.01585	$73.4 \pm 2.3 \pm 6.0$	$295 \pm 18_{-31}^{+36}$	$4.22 \pm 0.17_{-0.12}^{+0.31}$
110-130	$\mu^+\mu^-$	842	45	5	0.265	0.01202	$86.7 \pm 3.2 \pm 6.5$	$356 \pm 25_{-50}^{+35}$	$4.28 \pm 0.20_{-0.28}^{+0.16}$
130-150	$\mu^+\mu^-$	541	48	2	0.176	0.009331	$104 \pm 5 \pm 11$	$430 \pm 42_{-42}^{+60}$	$4.46 \pm 0.27_{-0.14}^{+0.28}$
150-170	$\mu^+\mu^-$	171	29	6	0.0586	0.007367	$110 \pm 11 \pm 12$	$488 \pm 84_{-35}^{+80}$	$4.58 \pm 0.41_{-0.16}^{+0.33}$
20-35	$e^+e^-$	982	216	16	0.087	0.06408	$33.6 \pm 1.6_{-2.4}^{+2.2}$	$128 \pm 16_{-16}^{+16}$	$3.55 \pm 0.27_{-0.14}^{+0.25}$
35-50	$e^+e^-$	2681	881	49	0.270	0.03730	$43.8 \pm 2.0_{-2.8}^{+2.9}$		
50-60	$e^+e^-$	1978	372	30	0.386	0.01791	$57.2 \pm 1.8_{-3.5}^{+3.6}$	$228 \pm 17_{-19}^{+35}$	$3.86 \pm 0.18_{-0.17}^{+0.35}$
60-70	$e^+e^-$	1821	408	35	0.383	0.01447	$62.5 \pm 2.3_{-3.9}^{+4.1}$		
70-80	$e^+e^-$	1577	326	30	0.371	0.01200	$68.9 \pm 2.6_{-4.5}^{+4.5}$	$258 \pm 26_{-25}^{+45}$	$3.98 \pm 0.23_{-0.22}^{+0.43}$
80-90	$e^+e^-$	1420	306	30	0.373	0.01013	$72.1 \pm 2.9_{-4.5}^{+4.9}$		
90-110	$e^+e^-$	2499	445	35	0.382	0.01620	$81.9 \pm 2.3_{-4.8}^{+4.9}$	$360 \pm 31_{-34}^{+58}$	$4.48 \pm 0.22_{-0.24}^{+0.45}$
110-125	$e^+e^-$	1604	235	21	0.371	0.00954	$95.7 \pm 3.2_{-5.4}^{+5.4}$		
125-140	$e^+e^-$	1470	221	14	0.378	0.00790	$103.9 \pm 3.6_{-5.8}^{+6.0}$	$439 \pm 38_{-35}^{+57}$	$4.30 \pm 0.19_{-0.17}^{+0.31}$
140-170	$e^+e^-$	2303	393	46	0.334	0.01218	$115.0 \pm 3.3_{-6.7}^{+7.7}$		
170-200	$e^+e^-$	1362	212	23	0.250	0.00877	$129.1 \pm 4.7_{-7.7}^{+8.1}$	$578 \pm 57_{-76}^{+72}$	$4.65 \pm 0.20_{-0.21}^{+0.28}$
200-230	$e^+e^-$	1161	261	19	0.243	0.00643	$141.7 \pm 6.1_{-8.7}^{+8.8}$		
230-260	$e^+e^-$	1208	442	13	0.280	0.00482	$140.3 \pm 7.4_{-9.9}^{+15.1}$	$557 \pm 120_{-93}^{+88}$	$4.05 \pm 0.38_{-0.25}^{+0.33}$
260-290	$e^+e^-$	1490	785	18	0.248	0.00369	$189 \pm 13_{-26}^{+15}$		

**Table 1:** *Measurements, in different ranges of  $W$ , of the total  $J/\psi$  photoproduction cross section, of the differential cross section extrapolated to  $t = 0$  and of the slope parameter  $b$  of the exponential  $t$  dependence. The first uncertainties are statistical and the second are systematic.  $N_{obs}$  is the number of events in the signal mass region,  $N_{non-res}$  is the estimated non-resonant background,  $N_{\psi(2S)}$  is the number of  $\psi(2S)$  events in the  $J/\psi$  mass region and  $\mathcal{A}$  is the acceptance. The effective photon flux,  $\Phi$ , is used to compute the  $\gamma p$  cross section from the  $ep$  cross section.*

Quantity	$J/\psi \rightarrow \mu^+\mu^-$	$J/\psi \rightarrow e^+e^-$	Method
$\delta$	$0.67 \pm 0.03 \pm 0.05$	$0.695 \pm 0.021 \pm 0.028$	Fits to
$W$ range	$30 < W < 170$ GeV	$35 < W < 290$ GeV	$\sigma \propto (W/90\text{GeV})^\delta$
$b_0$ (GeV $^{-2}$ )	$4.23 \pm 0.07^{+0.10+0.085}_{-0.12-0.051}$	$4.11 \pm 0.08^{+0.08+0.33}_{-0.09-0.16}$	Fits to
$\alpha'_{\mathcal{P}}$ (GeV $^{-2}$ )	$0.098 \pm 0.037 \pm 0.040 \pm 0.001$	$0.128 \pm 0.037^{+0.008}_{-0.025} \pm 0.005$	Eq. (2)
$\alpha_{\mathcal{P}}(0)$	$1.198 \pm 0.011 \pm 0.015$	$1.204 \pm 0.016^{+0.004}_{-0.013}$	Fits to
$\alpha'_{\mathcal{P}}$ (GeV $^{-2}$ )	$0.099 \pm 0.023 \pm 0.020$	$0.136 \pm 0.031^{+0.008}_{-0.020}$	Eq. (1)
$t$ range	$-t < 1.8$ GeV $^2$	$-t < 1.25$ GeV $^2$	

**Table 2:** Measurements of  $\delta$ ,  $b_0$ ,  $\alpha'_{\mathcal{P}}$  and  $\alpha_{\mathcal{P}}(0)$  obtained separately from the muon and electron decay channels. The first uncertainties are statistical and the second are systematic. Where given, the third refers to the modelling of the proton-dissociative subtraction. The last column indicates how the values were determined.

$t$ (GeV $^2$ )	Mode	$\alpha_{\mathcal{P}}(t)$
-0.079	$\mu^+\mu^-$	$1.188 \pm 0.011^{+0.010}_{-0.020}$
-0.28	$\mu^+\mu^-$	$1.172 \pm 0.016^{+0.010}_{-0.020}$
-0.48	$\mu^+\mu^-$	$1.161 \pm 0.023^{+0.015}_{-0.016}$
-0.68	$\mu^+\mu^-$	$1.100 \pm 0.028^{+0.030}_{-0.017}$
-0.92	$\mu^+\mu^-$	$1.143 \pm 0.028^{+0.015}_{-0.030}$
-1.34	$\mu^+\mu^-$	$1.032 \pm 0.040^{+0.030}_{-0.060}$
-0.10	$e^+e^-$	$1.189 \pm 0.018^{+0.005}_{-0.009}$
-0.35	$e^+e^-$	$1.153 \pm 0.014^{+0.006}_{-0.014}$
-0.68	$e^+e^-$	$1.127 \pm 0.019^{+0.012}_{-0.011}$
-1.05	$e^+e^-$	$1.044 \pm 0.029^{+0.021}_{-0.009}$

**Table 3:** Values of  $\alpha_{\mathcal{P}}(t)$  obtained from fits to the function  $d\sigma/dt \propto W^{4[\alpha_{\mathcal{P}}(t)-1]}$ . The first uncertainty is statistical and the second is the systematic.

# ZEUS

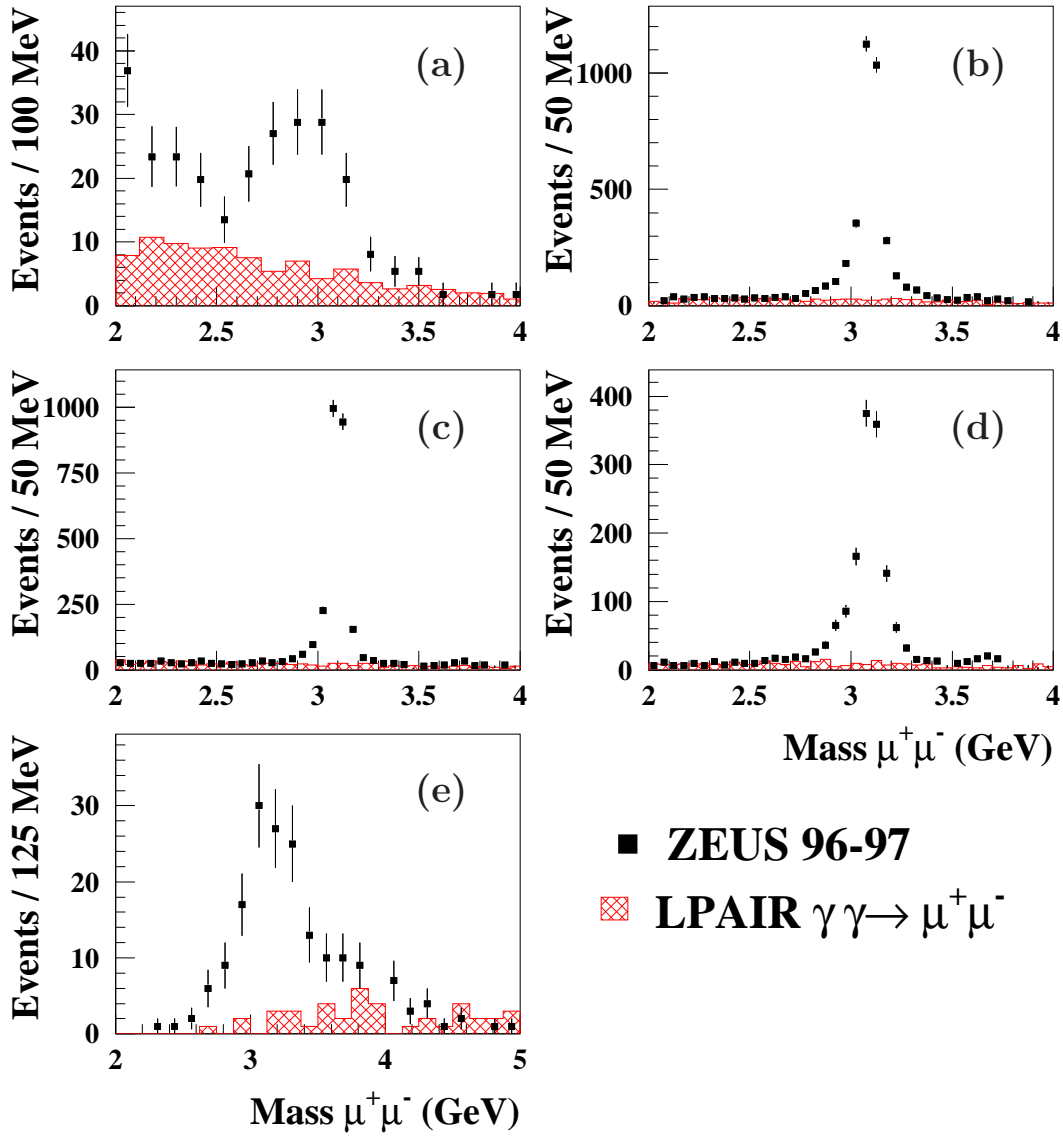


**Figure 1:** Invariant-mass distributions of the  $\mu^+\mu^-$  pairs in the different  $W$  regions: (a)  $20 < W < 30$  GeV, (b)  $30 < W < 70$  GeV, (c)  $70 < W < 110$  GeV, (d)  $110 < W < 150$  GeV and (e)  $150 < W < 170$  GeV. The histograms represent the LPAIR distributions of the non-resonant background.



# ZEUS

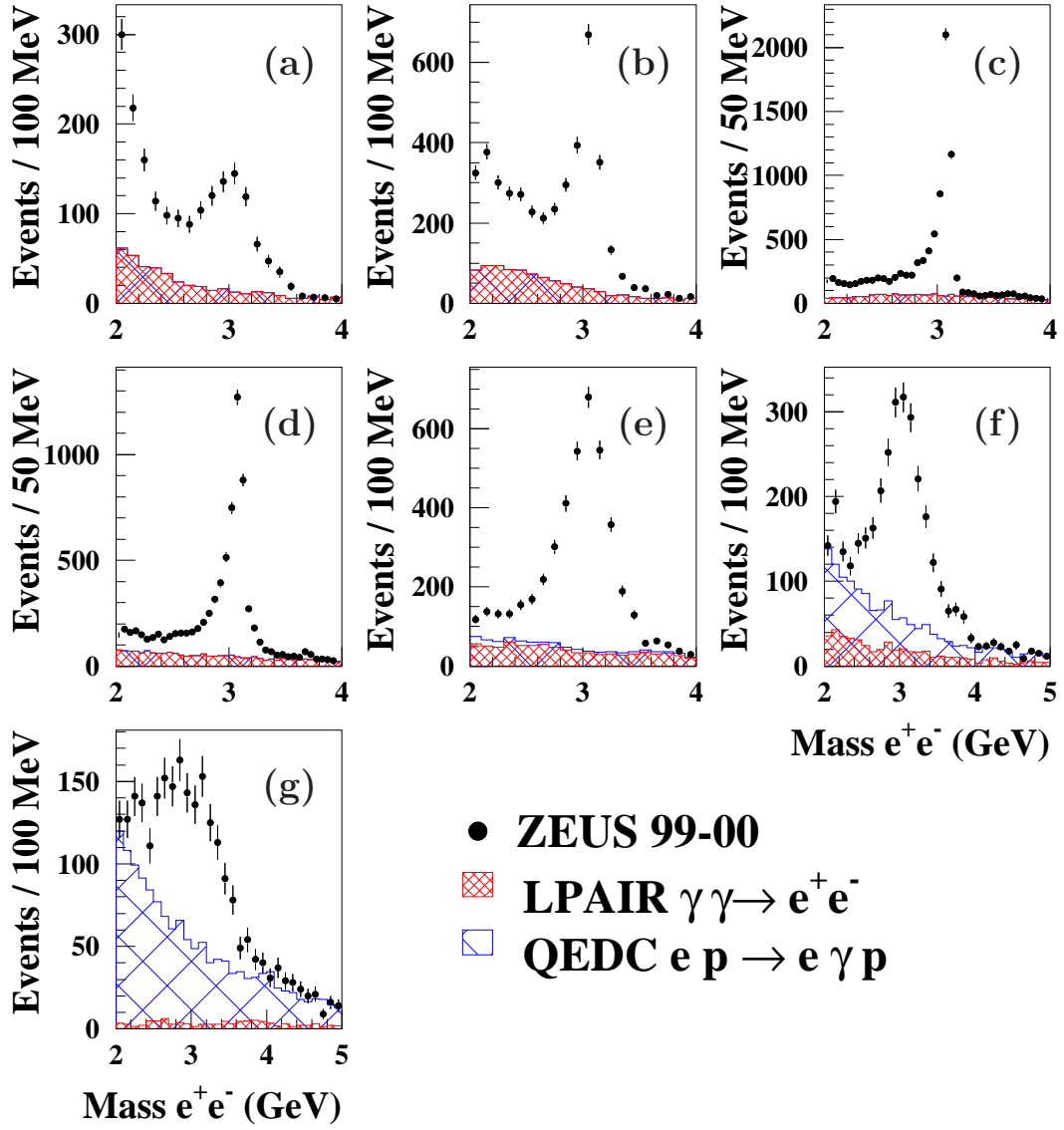


**Figure 2:** Invariant-mass distributions of the  $e^+e^-$  pairs in the different  $W$  regions: (a)  $20 < W < 35$  GeV, (b)  $35 < W < 50$  GeV, (c)  $50 < W < 90$  GeV, (d)  $90 < W < 140$  GeV, (e)  $140 < W < 200$  GeV, (f)  $200 < W < 260$  GeV and (g)  $260 < W < 290$  GeV. The close-hatched histogram represents the LPAIR Monte Carlo distribution for the non-resonant background and the wide-hatched histogram that from COMPTON2.

# ZEUS

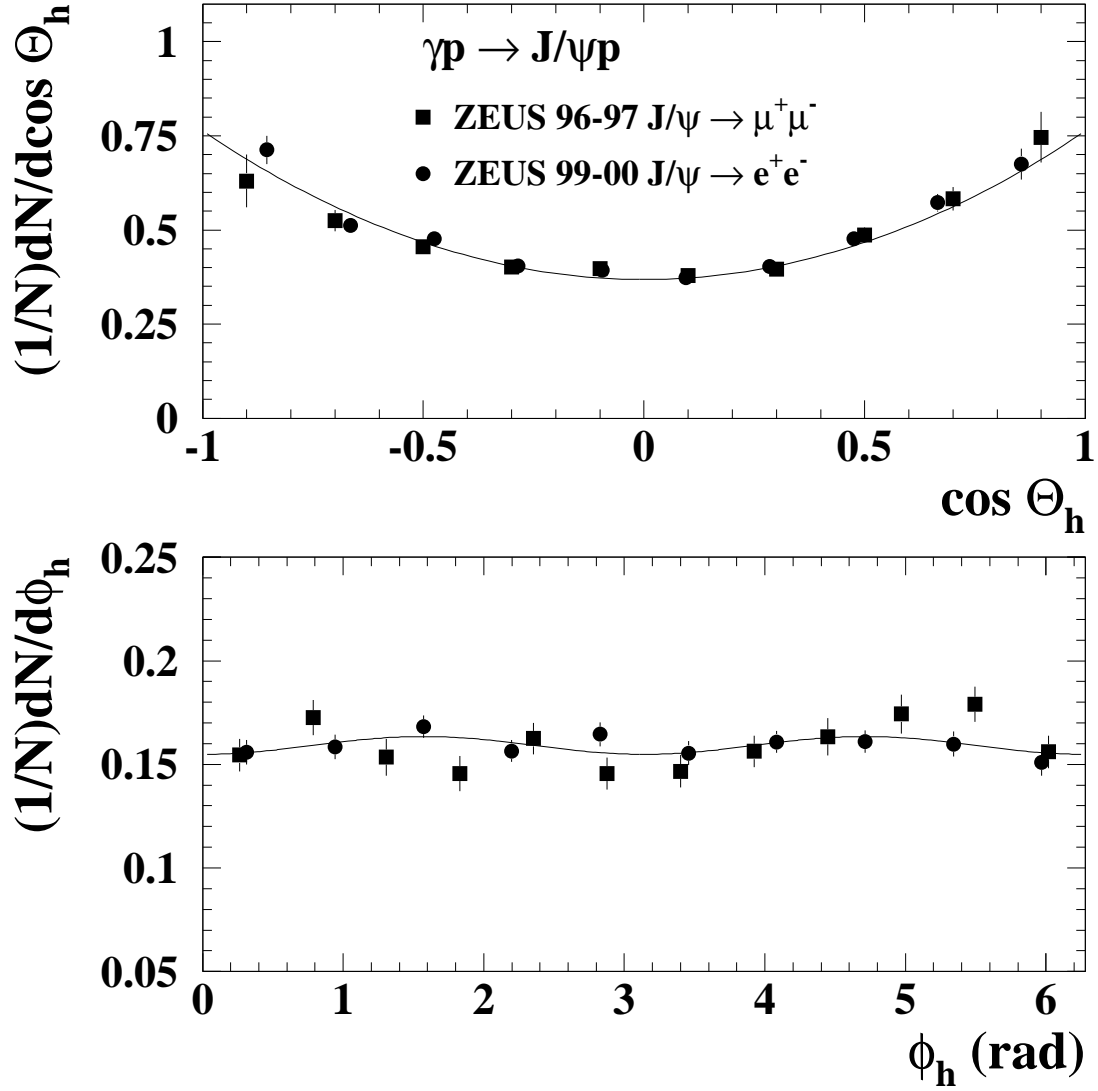


**Figure 3:** The acceptance-corrected decay angular distributions for exclusive  $J/\psi$  photoproduction in the kinematic range  $30 < W < 170 \text{ GeV}$  and  $|t| < 1 \text{ GeV}^2$ . The non-resonant background has been subtracted. The results of both the  $\mu^+\mu^-$  and  $e^+e^-$  decay channels are presented. The vertical bars indicate the statistical uncertainties only. The curves are the results of the fits to Eqs. (3) and (4), as described in the text.

# ZEUS

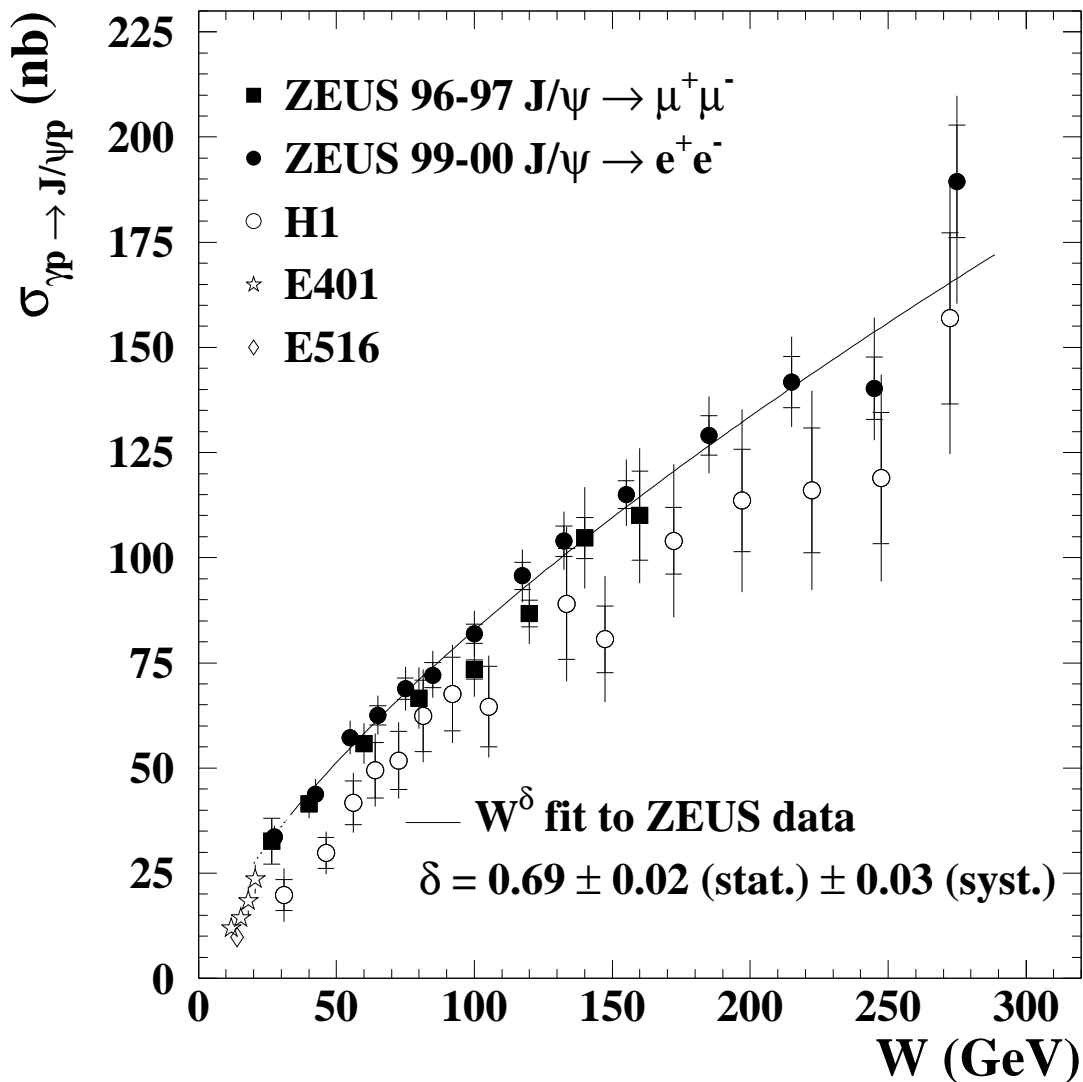


**Figure 4:** The exclusive  $J/\psi$  photoproduction cross section as a function of  $W$  for  $J/\psi \rightarrow \mu^+\mu^-$  and  $J/\psi \rightarrow e^+e^-$ . The inner bars indicate the statistical uncertainties; the outer bars are the statistical and systematic uncertainties added in quadrature. Results from the H1 [15], E401 [44] and E516 [45] experiments are also shown. The solid line is the result of a fit to the ZEUS data of the form  $\sigma \propto (W/90 \text{ GeV})^\delta$  and the dotted line is the extrapolation of the fit.

# ZEUS

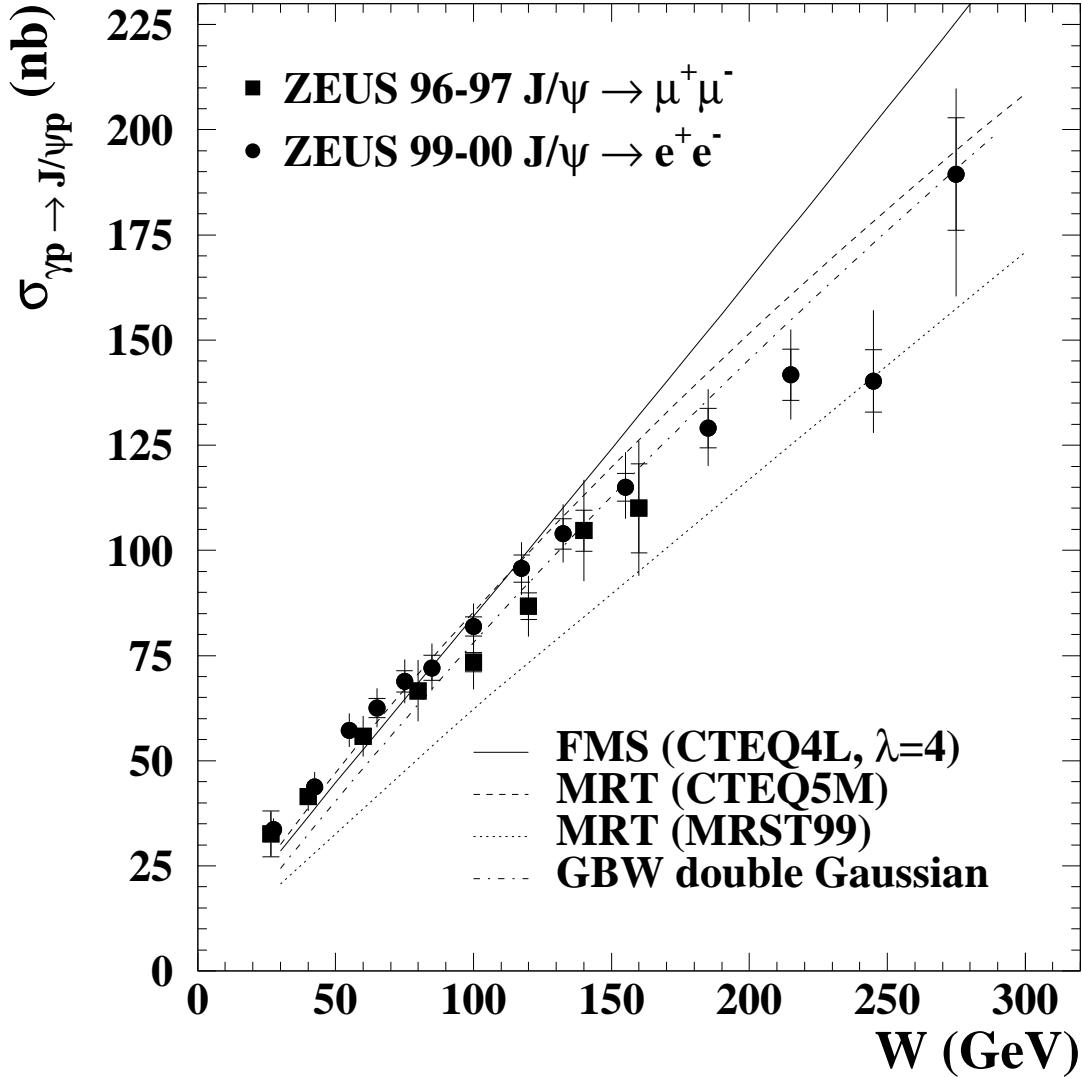


**Figure 5:** The exclusive  $J/\psi$  photoproduction cross section as a function of  $W$  obtained in the two leptonic decay channels,  $J/\psi \rightarrow \mu^+ \mu^-$  and  $J/\psi \rightarrow e^+ e^-$ . The inner bars indicate the statistical uncertainties, the outer bars are the statistical and systematic uncertainties added in quadrature. The experimental results are compared to the QCD predictions of MRT [5], using two different parameterisations of the gluon PDF in the proton, MRST99 [48] (dotted curve) and CTEQ5M [47] (dashed curve). The solid curve shows the QCD prediction of FMS [6] using  $\lambda = 4$  and the CTEQ4L [50] PDF. The dash-dotted curve displays the prediction [52] based on the colour-dipole model [53] with a double-Gaussian  $J/\psi$  wave-function; this prediction was re-scaled to the  $b$ -slope measured in this paper.

# ZEUS

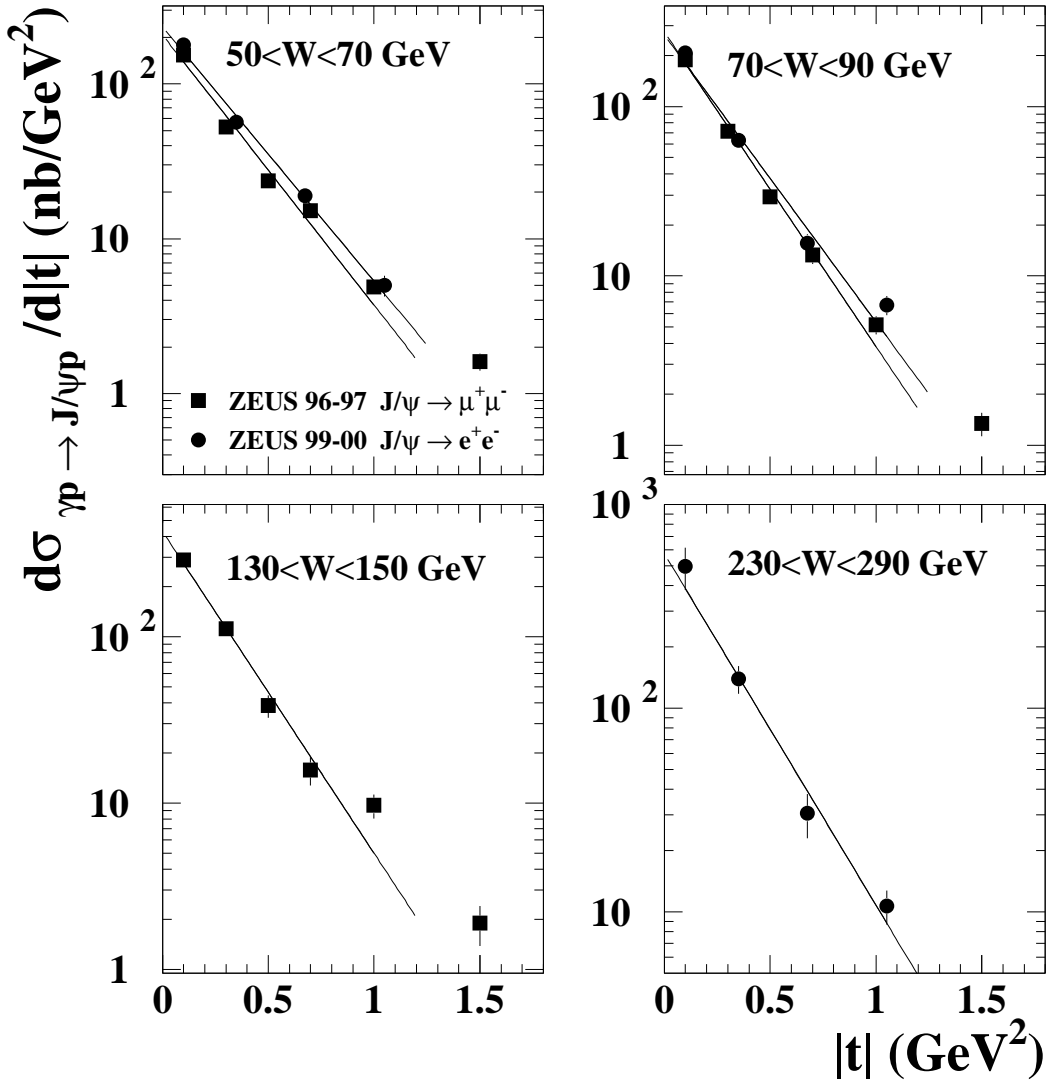


**Figure 6:** The differential cross-section  $d\sigma_{\gamma p \rightarrow J/\psi p}/dt$  for exclusive  $J/\psi$  photoproduction for representative bins of  $W$  and for the decay channels,  $J/\psi \rightarrow \mu^+\mu^-$  (squares) and  $J/\psi \rightarrow e^+e^-$  (points). The vertical bars indicate the statistical uncertainties only. The full lines represent the results of a fit of the form  $d\sigma/dt = d\sigma/dt|_{t=0} \cdot e^{bt}$  performed in the range  $-t < 1.2 \text{ GeV}^2$  for the muon channel and in the range  $-t < 1.25 \text{ GeV}^2$  for the electron channel.

# ZEUS

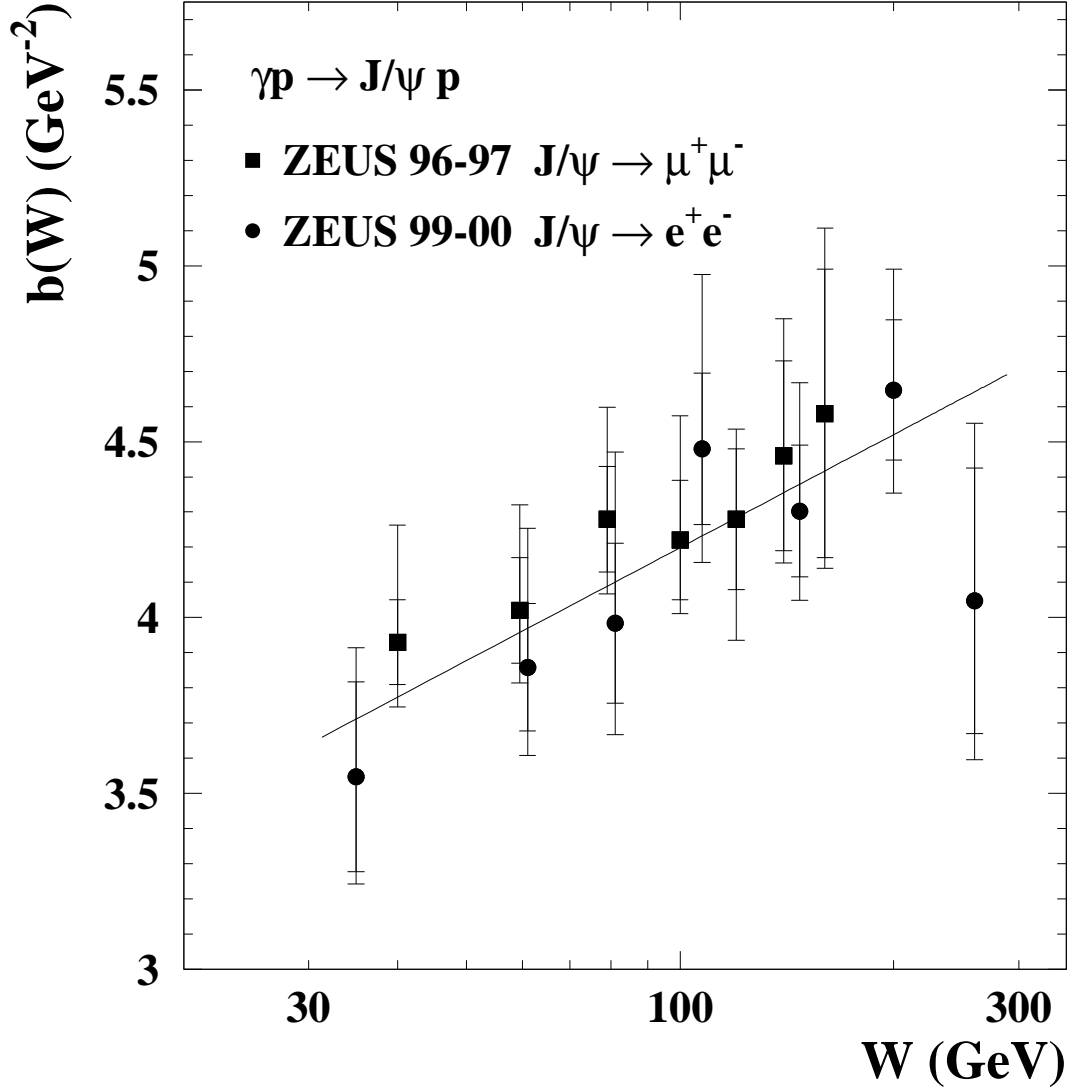


**Figure 7:** Values of the slope,  $b$ , of the  $t$  distribution, plotted as a function of  $W$ . The line shows the result of a fit of the form  $b(W) = b(90 \text{ GeV}) + 4 \cdot \alpha'_P \ln(W/90 \text{ GeV})$ .

# ZEUS

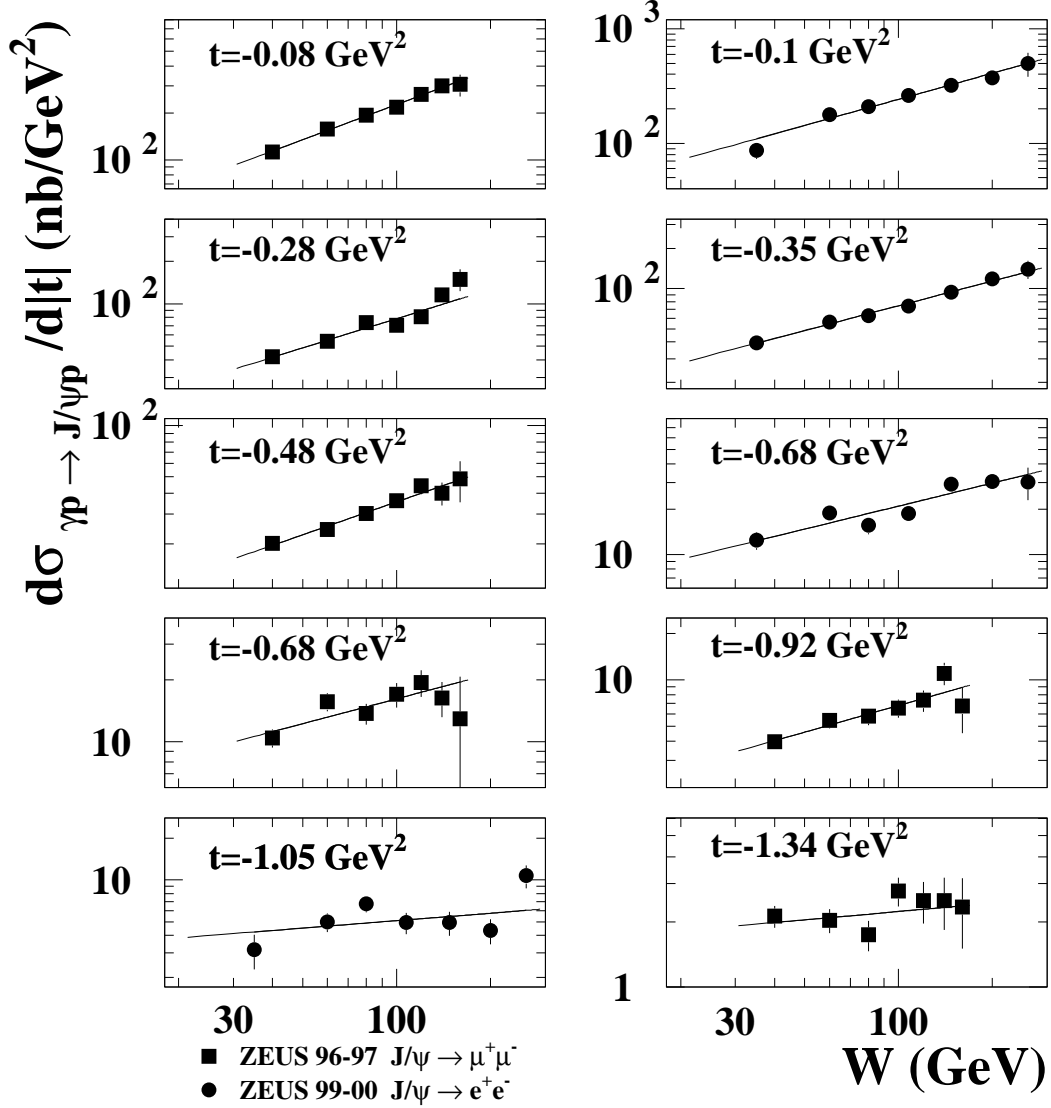


**Figure 8:** The differential cross-section  $d\sigma_{\gamma p \rightarrow J/\psi p} / dt$  as a function of  $W$  at fixed  $t$  values. Only the statistical uncertainties are shown. The lines correspond to the results of fits of the form  $d\sigma_{\gamma p \rightarrow J/\psi p} / dt \propto W^{4[\alpha_P(t)-1]}$ .

# ZEUS

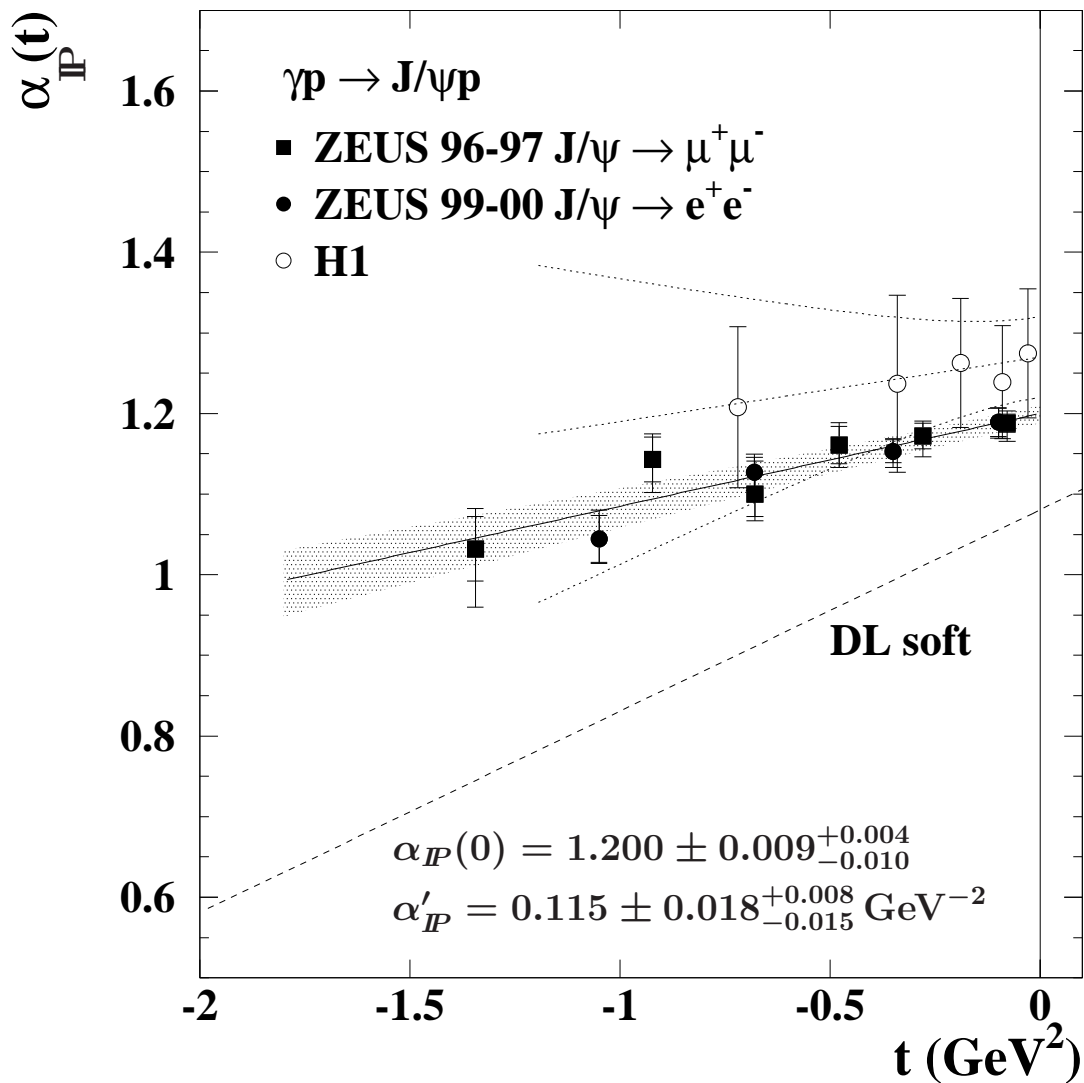


**Figure 9:** Pomeron trajectory as a function of  $t$  as obtained in the two leptonic decay channels,  $J/\psi \rightarrow \mu^+\mu^-$  and  $J/\psi \rightarrow e^+e^-$ . The inner bars indicate the statistical uncertainties; the outer bars are the statistical and systematic uncertainties added in quadrature. The results from the H1 Collaboration [15] are also shown. The solid and dotted lines are the result of linear fits to the ZEUS and H1 data, respectively. The one standard deviation contour is indicated for the ZEUS (shaded area) and H1 (dotted lines) measurements. The dashed line shows the DL soft-Pomeron trajectory [55].